TURUN
YLIOPISTO
UNIVERSITY
OF TURKU

TARGETED DELIVERY OF MOLECULAR SPHERICAL NUCLEIC ACIDS

Antti Äärelä

TURUN YLIOPISTON JULKAISUJA – ANNALES UNIVERSITATIS TURKUENSIS
SARJA – SER. AI OSA – TOM. 698 | ASTRONOMICA – CHEMICA – PHYSICA – MATHEMATICA | TURKU 2023

TURUN
YLIOPISTO
UNIVERSITY
OF TURKU

TARGETED DELIVERY OF MOLECULAR SPHERICAL NUCLEIC ACIDS

Antti Äärelä

TURUN YLIOPISTON JULKAISUJA – ANNALES UNIVERSITATIS TURKUENSIS
SARJA – SER. AI OSA – TOM. 698 | ASTRONOMICA - CHEMICA - PHYSICA – MATHEMATICA | TURKU 2023

University of Turku

Faculty of Science
Chemistry
Chemistry
Drug Research Doctoral Programme

Supervised by

Professor Pasi Virta
Department of Chemistry
University of Turku
Turku, Finland

Doctor Harri Salo
R&D, Orion Pharma
Turku, Finland

Doctor Olli Törmäkangas
R&D, Orion Pharma
Turku, Finland

Reviewed by

Professor Poul Nielsen
Department of Physics,
Chemistry and Pharmacy
University of Southern Denmark
Odense, Denmark

Professor Jørgen Kjems
Department of Molecular Biology and Genetics
Aarhus University
Aarhus, Denmark

Opponent

Professor Mauri Kostiainen
Department of Bioproducts and Biosystems
Aalto University
Espoo, Finland

ISBN 978-951-29-9425-0 (Print)
ISBN 978-951-29-9426-7 (Online)
ISSN 0082-7002 (Print)
ISSN 2343-3175 (Online)
Painosalama, Turku, Finland 2023

Perheelle ja ystäville

UNIVERSITY OF TURKU
Faculty of Science
Department of Chemistry
Chemistry
ANTTI ÄÄRELÄ: Targeted delivery of molecular spherical nucleic acids
Doctoral Dissertation, 122 pp.
Drug Research Doctoral Programme
September 2023

ABSTRACT

During the last decades, oligonucleotides (ONs) have emerged as an alternative therapeutic modality for a variety of diseases. They can target disease mechanisms that are considered undruggable by small molecular drugs and, in comparison to small molecular drug development, they can be developed rapidly from target identification to clinical use. However, their therapeutic potential is hindered by rapid renal clearance, widespread biodistribution, and poor cellular uptake. Spherical nucleic acids (SNAs) are an alternative covalent formulation for the delivery of therapeutic ONs. They are large enough to avoid renal clearance and are readily taken up to various cell types. Despite many beneficial properties their targeted systemic delivery remains a challenge. Tissue specific ligands can be utilized to facilitate targeted delivery but commonly used methodologies for SNA synthesis provide poor control over the valency and site of ligand attachment.

In this thesis, a controlled synthesis to obtain conjugates of well-defined [60]fullerene-based molecular SNAs (MSNAs) is described. The developed two-step assembly allows heterofunctionalization of MSNAs which can be utilized for site-specific ligand and labelling group integration. Various analytical methods were deployed to confirm the structural integrity and homogeneity of the synthesized MSNAs. Applicability of the MSNAs for site-specific radiolabelling was demonstrated and the effect of backbone chemistry, ligand decoration, and degree of labelling on the biodistribution was studied by positron emission tomography/computed tomography (PET/CT). The developed synthesis strategy was also applied for preparation of site-specific conjugates of glycan engineered antibodies (Ab) and MSNAs. Antigen binding properties, Ab-mediated endocytosis, and anti-proliferative effects of the conjugates on breast carcinoma cells were studied. Also, isopeptide bond formation between a peptide-ON conjugate and a recombinant protein was studied as an alternative methodology for generating Ab-ON conjugates (AOCs). The synthetic methodologies developed in this thesis can be used in the development of novel site-specific Ab-MSNA conjugates for diagnostic and therapeutic applications.

KEYWORDS: oligonucleotide, spherical nucleic acid, targeted delivery, antibody-oligonucleotide conjugate, radiolabelling, PET

TURUN YLIOPISTO
Matemaattis-luonnontieteellinen tiedekunta
Kemian laitos
Kemia
ANTTI ÄÄRELÄ: Molekulaaristen pallonukleiinihappojen kohdennettu lääkeainekuljetus
Väitöskirja, 122 s.
Lääketutkimuksen tohtoriohjelma
Syyskuu 2023

TIIVISTELMÄ

Viime vuosikymmeninä oligonukleotidit ovat nousseet esiin vaihtoehtoisena hoitomuotona useisiin sairauksiin. Niitä voidaan kohdistaa tautimekanismeihin, joihin pienmolekyylilääkkeet eivät sovellu, ja niiden kehitys kohteen tunnistamisesta kliiniseen käyttöön on nopeaa. Oligonukleotidien terapeuttista potentiaalia haittaavat kuitenkin nopea munuaissuodatus, laajalle levinnyt biodistribuutio ja huono soluunotto. Pallonukleiinihapot ovat terapeuttisten oligonukleotidien vaihtoehtoinen kovalenttinen formulaatio. Ne ovat riittävän suuria välttääkseen munuaissuodatuksen, ja ne otetaan helposti sisään erilaisiin solutyyppeihin. Monista hyödyllisistä ominaisuuksista huolimatta niiden haasteena on kohdennettu lääkeainekuljetus systeemisessä annostelussa. Kudosspesifisiä ligandeja voidaan käyttää parantamaan kohdennettua lääkeainekuljetusta, mutta yleisimmin käytetyt pallonukleiinihappojen synteesimenetelmät eivät mahdollista ligandien tai leima-aineiden paikkaspesifistä liittämistä.

Tässä väitöskirjassa kuvataan [60]fullereenipohjaisten molekulaarisesti määriteltyjen pallonukleiinihappojen valmistusmenetelmä, joka mahdollistaa paikkaspesifisen ligandien ja leimausryhmien liittämisen osaksi rakennetta. Valmistettujen rakenteiden oikeellisuus ja yhteneväisyys varmistettiin useilla analyyttisillä menetelmillä. Pallonukleiinihapot radioleimattiin paikkaspesifisesti, ja oligonukleotidin selkärangan kemian, ligandikoristelun ja leimausasteen vaikutusta biodistribuutioon tutkittiin positroniemissiotomografialla/tietokonetomografialla (PET/CT). Työssä kuvataan myös glykaanimuokattujen vasta-aineiden ja pallonukeiinihappojen paikkaspesifisien konjugaattien valmistus. Lisäksi tutkittiin valmistettujen konjugaattien sitoutumisominaisuuksia kohdeantigeeniin, vasta-ainevälitteistä soluunottoa ja vaikutusta rintasyöpäsolujen kasvuun. Myös isopeptidisidoksen muodostumista peptidi-oligonukleotidikonjugaatin ja rekombinanttiproteiinin välillä tutkittiin vaihtoehtoisena menetelmänä vasta-aine-oligonukleotidikonjugaattien valmistamiseen. Kehitettyjä synteettisiä menetelmiä voidaan käyttää uudenlaisten paikkaspesifisten pallonukleiinihappojen ja vasta-aineiden yhdistelmärakenteiden kehittämisessä diagnostisiin ja terapeuttisiin sovelluksiin.

ASIASANAT: oligonukleotidi, pallonukleiinihappo, lääkeainekuljetus, vasta-aineoligonukleotidikonjugaatti, radioleimaus, PET

Table of Contents

Abbreviations

Ab	antibody
AF488	Alexa Fluor 488 (fluorescent dye)
AGO2	argonaute 2 protein
AGTR1	angiotensin type 1 receptor
AIDS	acquired immune deficiency syndrome
AOC	antibody-oligonucleotide conjugate
AP	alkaline phosphatese
apoB	apolipoprotein B
AR-V7	androgenic receptor variant
ASGR1	asialoglycoprotein receptor 1
ASO	antisense oligonucleotide
BBB	blood-brain barrier
BCN	bicyclo[6.1.0]non-4-yne
BLI	biolayer interferometry
cEt	constrained ethyl DNA
CNS	central nervous system
CPP	cell-penetrating peptide
Cy5	Cyanine5 (fluorescent dye)
DBCO	dibenzocyclooctyne
DBU	1,8-diazabicyclo[5,4,0]undec-7-ene
DCM	dichloromethane
DLS	dynamic light scattering
DMSO	dimethyl sulfoxide
DNA	deoxyribonucleic acid
DNase	deoxyribonuclease
DOTA	1,4,7,10-tetraazacyclododecane1,4,7,10-tetraacetic acid
E2	17β-estradiol
EDTA	ehylenediaminetetraacetic acid
EPR	enhanced permeability and retention
ESI-TOF	electrospray ionization time-of-flight mass spectroscopy
FDA	Food and Drug Administration (USA)

FDG	2-deoxy-2-fluoro-*D*-glucose
FMT-CT	fluorescence molecular tomography fused with computed tomography
GalNAc	*N*-Acetylgalactosamine
GlcNAc	*N*-acetylglucosamine
HER2	human epidermal growth factor receptor 2
iEDDA	inverse electron-demand Diels-Alder reaction
IgG	immunoglobulin G
immuno-PCR	immuno-polymerase chain reaction
LNA	locked nucleic acid
MC-LR	microcystin-LR
MFI	median fluorescence intensity
miRNA	microRNA
MPS	mononuclear phagocyte system
mRNA	messenger RNA
MS	mass spectrometry
MSNA	molecular spherical nucleic acid
NHS	*N*-hydroxysuccinimide
Ni-NTA	Nickel-nitriloacetic acid
NIR-II	second near infrared window
ON	oligonucleotide
ONP	oligonucleotide nanoparticle
PAGE	polyacrylamide gel electrophoresis
PBS	phosphate buffered saline
PEG	polyethylene glycol
PET/CT	positron emission tomography/computed tomography
PMO	phosphorodiamidate morpholino oligomers
PNA	peptide nucleic acid
PO	phosphodiester
PS	phosphorothioate
PSMA	prostate-specific membrane antigen
RISC	RNA induced silencing complex
RNA	ribonucleic acid
RNase	ribonuclease
RNAi	RNA interference
RP HPLC	reversed phase high-performance liquid chromatography
scFv	single-chain variable fragment
SD	standard deviation
SEC	size-exclusion chromatography

SEC-MALS	size-exclusion chromatography equipped with multi-angle light scattering detector
SEM	standard error of the mean
siRNA	small interfering RNA
SNA	spherical nucleic acid
SPAAC	strain promoted alkyne-azide cycloaddition
SPOS	solid-phase oligonucleotide synthesis
ssDNA	single strand DNA
SUV	standardized uptake value
tcDNA	tricyclo DNA
TCO	*trans*-cyclooctene
TEG	tetraethyleneglycol
TEM	transmission electron microscopy
TFA	trifluoroacetic acid
TLC	thin layer chromatography
TRFIA	time-resolved fluorescence immunoassay
Tz	tetrazine
UDP-GalNAz	*N*-azidoacetylgalactosamine
UV	ultraviolet

List of Original Publications

This dissertation is based on the following original publications, which are referred to in the text by their Roman numerals:

I Kushnarova-Vakal, A., Äärelä, A., Huovinen, T., Virta, P., and Lamminmäki U. Site-Specific Linking of an Oligonucleotide to Mono- and Bivalent Recombinant Antibodies with SpyCatcher-SpyTag System for Immuno-PCR *ACS Omega* **2020** 5 (38), 24927-24934.

II Gulumkar, V.*, Äärelä, A.*, Moisio, O., Rahkila, J., Tähtinen, V., Leimu, L., Korsoff, N., Korhonen, H., Poijärvi-Virta, P., Mikkola, S., Nesati, V., Vuorimaa-Laukkanen, E., Viitala, T., Yliperttula, M., Roivainen, A., and Virta, P. Controlled Monofunctionalization of Molecular Spherical Nucleic Acids on a Buckminster Fullerene Core *Bioconjugate Chemistry* **2021**, *32* (6), 1130-1138.

III Äärelä, A.*, Auchynnikava, T.*, Moisio, O., Liljenbäck, H., Andriana, P., Iqbal, I., Lehtimäki, J., Rajander, J., Salo, H., Roivainen, A., Airaksinen, A. J., and Virta, P. *In Vivo* Imaging of [60]Fullerene-Based Molecular Spherical Nucleic Acids by Positron Emission Tomography *Molecular Pharmaceutics* **2023**; Published ahead of print.

IV Äärelä, A., Räsänen, K., Holm, P., Salo, H., and Virta, P. Synthesis of Site-Specific Antibody-[60]Fullerene-Oligonucleotide Conjugates for Cellular Targeting *ACS Applied Bio Materials* **2023**, 6 (8), 3189–3198.

 *Equal contribution.

List of Contemporaneous Publications

Österlund, T., Aho, A., Äärelä, A., Tähtinen, V., Korhonen, H., and Virta, P. Immobilized Carbohydrates for Preparation of 3′-Glycoconjugated Oligonucleotides. *Current Protocols in Nucleic Acid Chemistry* **2020**, *83* (1), e122.

Aho, A., Äärelä, A., Korhonen, H., and Virta, P. Expanding the Scope of the Cleavable *N*-(Methoxy)oxazolidine Linker for the Synthesis of Oligonucleotide Conjugates. *Molecules* **2021**, *26* (2), 490.

Aro-Heinilä, A., Lepistö, A., Äärelä, A., Lönnberg, T., and Virta, P. 2-Trifluoromethyl-6-mercurianiline Nucleotide, a Sensitive ^{19}F NMR Probe for Hg(II)-mediated Base Pairing. *J. Org. Chem.* **2022**, *87* (1), 137–146.

Gulumkar, V., Tähtinen, V., Ali, A., Rahkila, J., Valle-Delgado, J. J., Äärelä, A., Österberg, M., Yliperttula, M., and Virta, P. Synthesis of an Azide- and Tetrazine-Functionalized [60]Fullerene and Its Controlled Decoration with Biomolecules. *ACS Omega* **2022**, *7* (1), 1329–1336

1 Introduction

1.1 Therapeutic oligonucleotides

Therapeutic oligonucleotides (ONs) are short, single- or double-stranded sequences typically composed of 15-150 nucleotides, designed to modulate gene expression, or block the activity of specific genes, proteins, or small molecules.[1,2] They can be chemically synthesized[3] or produced by enzymatic means[4] and tailored to target specific regions of ribonucleic acid (RNA) or deoxyribonucleic acid (DNA) targets. They are typically administered via local or systemic injection.[5] High specificity to target nucleic acid sequences enables rational design based on knowledge of the primary sequence of a target gene which allows rapid development from target identification to first clinical dose in even less than a year.[6] Therapeutic oligonucleotides can be used to treat a variety of diseases, including genetic disorders, viral infections, and cancer. Disease-mechanism considered undruggable by small molecules could be targeted with ON therapeutics. Their principal action is based on binding, via complementary Watson-Crick base pairing (Figure 1), to their RNA targets, which prevents or modulates protein translation.[7] However, for some sequences the mode of action is via binding to specific target proteins or small molecules with high affinity and specificity to modulate their function in agonistic or antagonistic fashion.[8,9]

The first therapeutic ON, Fomivirsen (Ionis Pharma, later Novartis), was approved by the US Food and Drug Administration (FDA) in 1998.[10,11] It is a 21mer phosphorothioate (PS) DNA used in the treatment of cytomegalovirus retinitis in immunocompromised patients, including those with acquired immune deficiency syndrome (AIDS). It served a high unmet medical need in the days of its launch but was withdrawn by Novartis in 2000s due to reduced clinical use after developments of other in anti-viral therapies.[12] To date 15 therapeutic oligonucleotides have been approved by the FDA.[13]

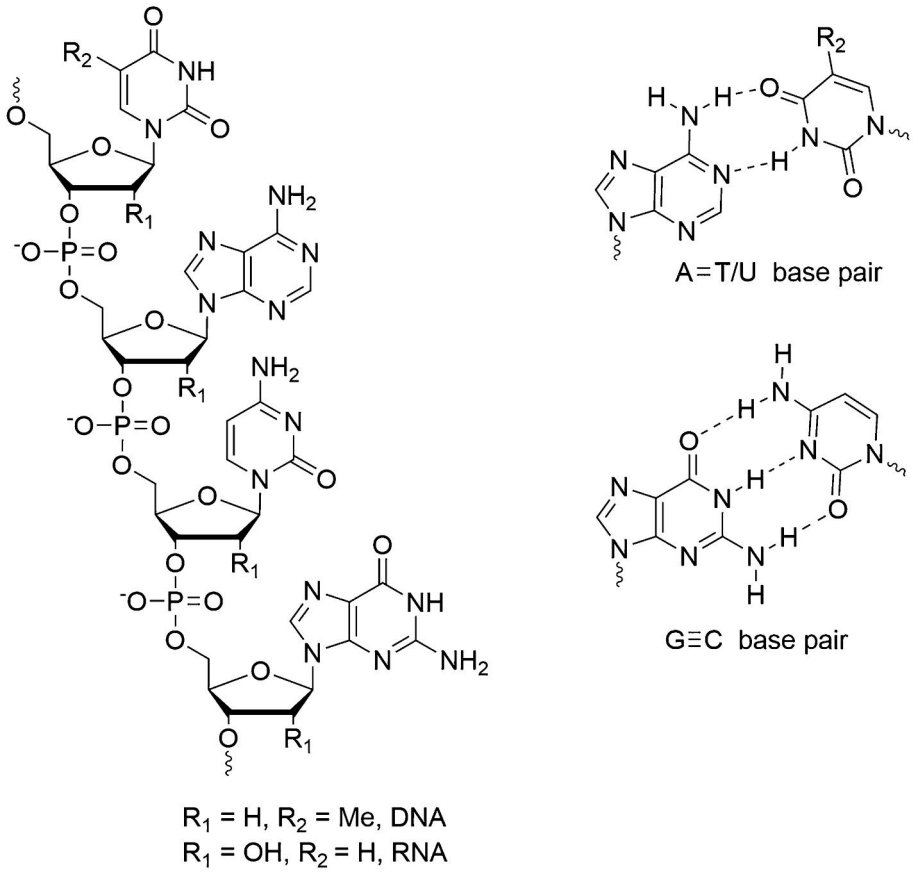

Figure 1. Structure of DNA and RNA, and Watson−Crick base pairing.

Different types of therapeutic oligonucleotides include antisense oligonucleotides (ASOs), small interfering RNA (siRNA), microRNA (miRNA) and aptamers (Figure 2). ASOs are designed to hybridize with specific mRNA molecules and inhibit their translation into proteins by inducing degradation of their target mRNA transcripts by RNAase H-activation, or by sterically blocking the translation.[14–16] By blocking the production of disease-causing proteins, antisense oligonucleotides can treat a range of genetic diseases, including cystic fibrosis and spinal muscular atrophy. The typical design for ASOs that are competent in RNase H in the current generation usually involves a "gapmer" pattern with central DNA-based gap surrounded by RNA-based flanking regions that are chemically modified to enhance target binding.[17] It is worth noting that RNase H1 exhibits activity in both the nucleus and cytoplasm, which enables the targeting of nuclear transcripts such as immature pre-mRNAs and long non-coding RNAs that may not be as accessible to alternative technologies like small molecules.[18,19]

Steric block oligonucleotides are a class of ASOs which contain nucleotides that do not form RNase H substrates when paired with RNA.[5] They are designed to bind to target transcripts and thereby interfere with transcript RNA–RNA and/or RNA–protein interactions. A common application of steric block ASOs is to alter splicing of precursor mRNA[20,21]. The goal of splicing modulation can be to restore the translational reading frame to induce production of a therapeutic protein (exon inclusion)[22,23], or to corrupt the splicing to reduce the translation of target gene (exon exclusion)[24].

Small interfering RNA (siRNA) is a double-stranded RNA molecule that targets specific mRNA molecules for degradation via RNA interference (RNAi) pathway. They typically possess a characteristic 19 + 2mer structure, consisting of a duplex composed of two 21-nucleotide RNA molecules with 19 complementary bases and 2-nucleotide 3′ overhangs at the termini.[25] One of the strands in the siRNA, known as the guide or antisense strand, is complementary to the target transcript, while the other strand is referred to as the passenger or sense strand. Complementarity between siRNA and its target transcript induces Argonaute 2 protein (AGO2) catalysed cleavage (slicer activity) of the target, resulting in gene silencing. AGO2 is part of the RNA-induced silencing complex (RISC), which is a ribonucleoprotein multiprotein complex that operates in gene silencing through various pathways involving both transcriptional and translational levels.[26–28]

MicroRNA is a type of small endogenous RNA that regulates gene expression by binding to specific mRNA molecules and inhibiting their translation into proteins. They are lucrative drug targets as they are associated with various physiological and pathophysiological processes, including cancer[29,30], cell cycle progression[31], infectious disease[32,33], immunity[34], diabetes[35], metabolism[36], myogenesis[37,38] and muscular dystrophy[39,40]. By targeting specific miRNAs, therapeutic oligonucleotides can modulate the expression of disease associated genes. Anti-miRNA oligonucleotides, also known as anti-miRs or antagomirs, have been widely employed as steric block ASOs to competitively hinder miRNAs by directly binding to the small RNA molecules within the RISC complex.[41,42] Steric block ASOs offer an alternative strategy for miRNA inhibition, by masking the target sequence on an mRNA transcript and inhibiting a specific miRNA regulatory interaction.[43,44]

Aptamers are nucleic acids which fold to three-dimensional structure able to bind to target proteins or small molecules with high affinity and specificity. They are often referred as chemical antibodies which underlines the difference of their mechanism of action compared to other therapeutic ONs.[9] They can be developed through iterative selection techniques[45,46], and their applicability against various targets have been demonstrated.[47–56] As an alternative oligonucleotide modality, they further widen the target scope of ON therapeutics.

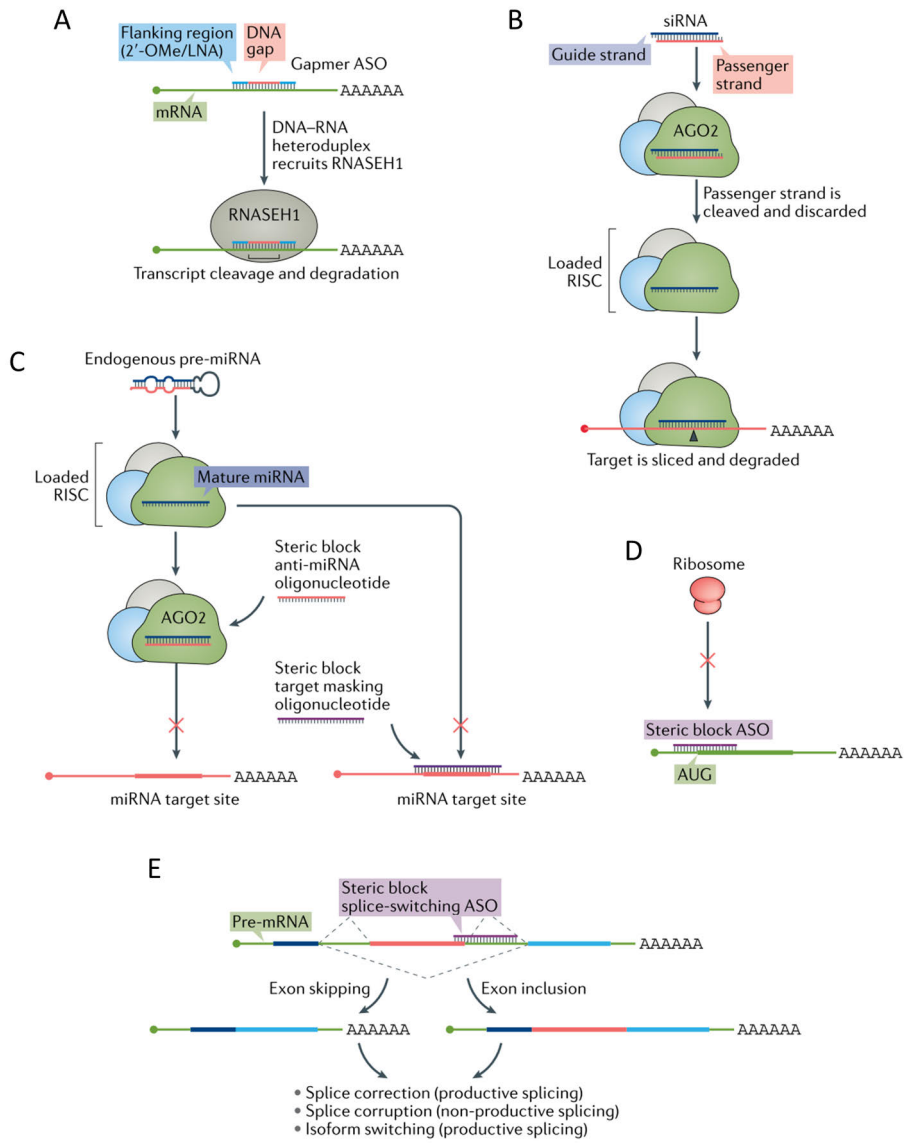

Figure 2. Mechanisms of action for threrapeutic ONs. A) Gapmer ASO B) siRNA C) anti-miRNA ON D) Steric block ASO E) Splice-switchin ASO. Adapted with permission from *Nat Rev Drug Discov*, 2020, 19, 673-694.

Therapeutic potential of ONs can be improved by various chemical modifications to enhance their stability, specificity, pharmacokinetic properties, and cellular uptake (Figure 3). Modifications can be indroduced to the sugar ring, phosphate backbone or nucleobases and typically are incorporated to the ON structure as modified building blocks in the nucleotide chain elongation. Commonly used sugar

modificatios are 2′-O-methyl (2′-OMe)[57,58], 2′-O-methoxy-ethyl (2′-MOE)[59] or 2′-fluoro (2′-F)[60] analogues of the ribonucleotides. They increase binding affinity to the target RNA and nuclease resistance. Locked nucleic acid (LNA)[61], tricyclo DNA (tcDNA)[62] and constrained ethyl DNA (cEt)[63] are constrained nucleotide analogues. These reduce the conformational flexibility of the nucleotides, favor A-form duplex formation and increase the binding affinity. As a drawback, the constrained analugues are incompatible with RNase H-mediated cleavage. In phosphorothioate (PS) modified ONs, one of the non-bridging oxygen atoms in the phosphate backbone is replaced with a sulfur atom. This enhances nuclease resistance and increases bioavailability by reducing renal clearance due to increased serum protein binding. However, the affinity towards the target RNA is typically reduced with PS modification.[64] The backbone chemistry can be also changed complitely to alter the charge and conformational flexibility of the ON. Peptide nucleic acid (PNA)[65] involves the replacement of the sugar-phosphate backbone with a polyamide, and in phosphorodiamidate morpholino oligomers (PMOs)[66] a 6-membered morpholino ring and phosphorodiamidate linkages are used. Like constrained analogues, PNA and PMO do not activate RNase H.

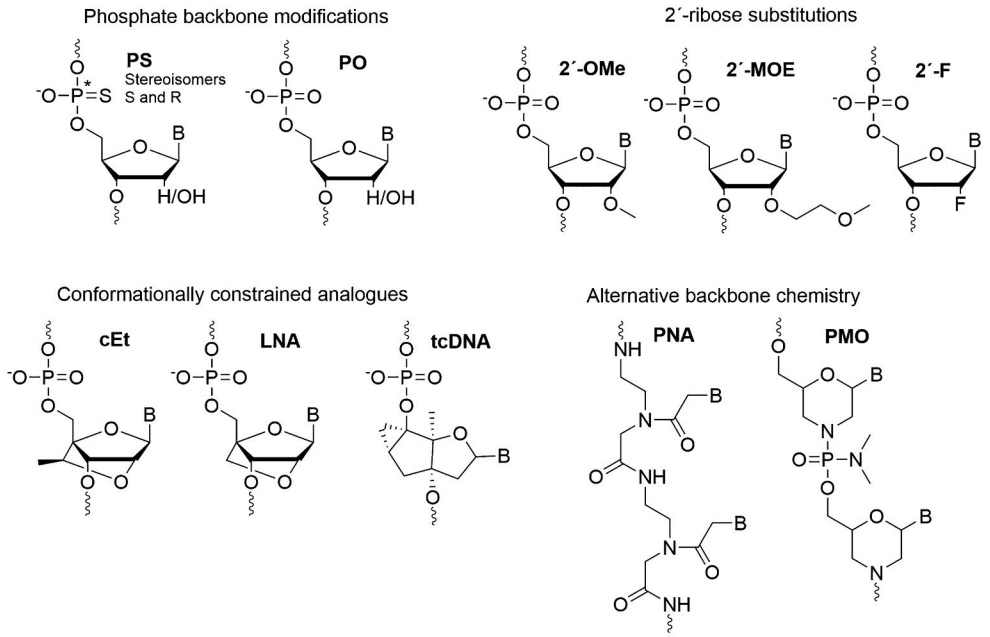

Figure 3. Chemical modifications of therapeutic ONs.

1.1.1 Challenges in oligonucleotide delivery

Successful delivery of ON therapeutics to their desired site-of-action is a significant hurdle. They, by no means, fit to the criteria of Lipinski´s rule of five for orally administrable therapeutics as ONs are large, hydrophilic polyanions, weighing typically 5-15 kDa, making them administrable only locally or through injection. In addition, these characteristics make it difficult for them to pass through the plasma membrane without additional carriers which significantly reduces their bioavailability.[2] To reach their target site-of-action, nucleic acid drugs must resist nuclease degradation in the extracellular space, bypass renal clearance, evade certain plasma proteins´ non-productive sequestration, and avoid removal by the reticuloendothelial system, including mononuclear phagocytes, liver sinusoidal endothelial cells, and Kupffer cells. Even if they reach their target organ, they must cross the capillary endothelium to reach the target cell within an organ, penetrate the plasma membrane, escape the endosome system before lysosomal degradation or re-export via exocytosis, and arrive at the correct intracellular site-of-action. Poor blood-brain barrier (BBB) penetration adds one more hurdle for systemic administration of central nervous system (CNS) targeting ONs.[2,16,67–70]

As other therapeutics, ONs can potentially bind to unintended targets, leading to off-target effects and toxicity.[71] Furthermore, they can elicit immune response in some patients, leading to unwanted side effects or decreased efficacy.[72] Careful design of the sequence minimizes the off-target effects, and in addition, nucleobase modifications[73,74] can be used to reduce immunogenicity. Latest well know example for successful deployment of non-canonical nucleobases are mRNA vaccines where uridine modifications played a significant role in suppression of immunogenic response.[75] The requirement for targeted systemic delivery can be in some cases bypassed by local administration. Approved ON therapeutics have been successfully administered locally by intravitreal or intrathecal routes, to treat eye and CNS conditions, respectively.[5] However, injection into these delicate organs is a highly invasive procedure which requires specialized training and equipment, and it can be associated with potential risks and severe complications. Although there are many options to improve therapeutic potential and reduce unwanted effects of ONs already in the current state, in cases where these principles are not applicable the look for possibility of systemic administration utilizing targeted delivery is in order.

1.2 Spherical nucleic acids

Spherical nucleic acids (SNAs) are a class of nucleic acid-based nanostructures with a spherical morphology. They consist of a radially ordered array of nucleic acid strands attached to the surface of a nanoparticle core e.g., gold[76–78], platinum[79], iron oxide[80], silver[81], silica[82], fullerene[82], or micelles[83–87] (Figure 4). The nucleic acid

strands are typically DNA or RNA sequences that are designed to interact with specific molecular targets, such as protein receptors or complementary nucleic acid sequences. The highly ordered arrangement of the nucleic acids on the nanoparticle surface gives SNAs many beneficial properties compared their linear counter parts: i) they are readily taken up by over 60 cell types[88], ii) muted innate immune responses[89], iii) resistance to nuclease degradation[82,90], and iv) are large enough to avoid renal clearance[85,91]. They have been shown to be highly effective at penetrating cell membranes and targeting intracellular molecules without additional carriers, making them attractive tools for studying cell biology and developing new therapies.[88,92,93] In addition to use as an alternative formulation for therapeutic ON delivery, SNAs can be utilized as delivery agents for small molecular drugs[94,95] and proteins[96,97].

1.2.1 Synthesis of SNAs

Typical methodologies for SNA synthesis produce polydisperse structures with unspecific valency of ONs as the typical number of ONs per particle varies from 30-150.[98–100] Gold-based SNAs are straight forward to synthesize utilizing thiol-modified ONs which readily bind to gold surfaces.[100] Another often used methodology relies on lipid modified ONs which in aqueous conditions form micelles with ONs on the outer sphere.[99] After sphere formation, the polyvalent products can be purified from single ONs using centrifugation or size-exclusion chromatography (SEC). Transmission electron microscopy (TEM), dynamic light scattering (DLS), and UV-Vis spectroscopy can be applied to confirm desired size, shape, and surface chemistry. Molecularly more defined structures have been synthesized around silica and fullerene nanoparticles utilizing strain-promoted alkyne-azide cycloaddition (SPAAC) between alkyne-modified ONs and azide-modified silsesquioxane and fullerene cores.[82] These molecular spherical nucleic acids (MSNAs) have lower ON valency compared to gold and lipid based particles; 8 and 12, for silsesquioxane and fullerene, respectively. The above-mentioned characterization techniques can be applied to these molecularly defined structures as well. Despite the lower ON valency, MSNAs retain carrier-free cellular uptake properties associated with larger polydisperse counterparts as well as the increased nuclease stability compared to linear ONs.

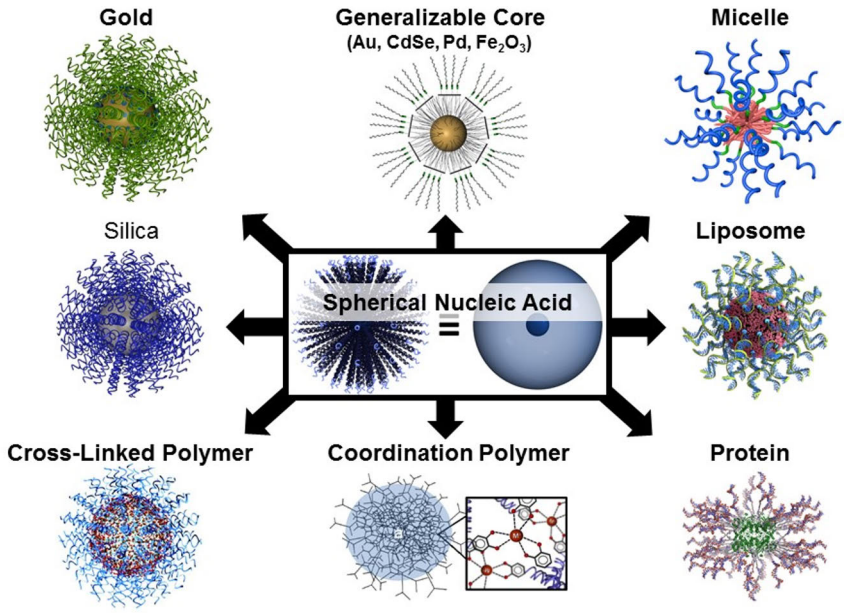

Figure 4. The structural versatility of SNAs. Reprinted with permission from https://mirkin-group.northwestern.edu/project/spherical-nucleic-acids/.

1.2.2 Biological properties of SNAs

Nuclease resistance properties of SNAs depend on the ON loading of the nanoparticle. *In vitro,* gold nanoparticle based SNAs loaded with native DNA have shown resistance towards DNase I and DNase II directly proportional to the ON loading as denser packing increased the stability. This phenomena can be seen also with the low valency MSNAs as 8-valency silsesquioxane based particles are more susceptible towards nucleases compared to 12-valency fullerene based particles.[82] As expected, when SNAs were loaded with PS modified ONs no enzymatic degradation was observed.[90]

Higher ON loading also positively affects the uptake of SNAs. SNAs interaction with scavenger receptors is dependent on the ON density of the nanoparticle. Increased Scavenger receptor mediated endocytosis is exhibited as the function of ON density.[98,101,102] Dense ON monolayer mimics the complex quadraplex-like structures of polyinosinic acid, a well-known ligand of the scavenger-receptor family.[103,104] When comparing internalization of SNAs in serum containing and serum free cell cultures, internalization has been elevated in the absence of serum proteins. This indicates that serum proteins act as competitive ligands binding to SNAs inhibiting the cellular uptake of SNAs.[101]

Although the spherical formulation brings many improved properties compared to the linear ONs, it makes the formulation more susceptible to delivery challenges

generally associated with nanoparticles. When nanoparticles are administered intravenously, they face a series of biological barriers that hinder their effective and targeted delivery to their site-of-action.[105] The first obstacle is opsonization, binding of plasma proteins, which leads to uptake by macrophages of the mononuclear phagocyte system (MPS) and high accumulation in organs like the spleen and liver, causing non-specific distribution to healthy organs.[106,107] Important factor is also the distance from the endothelial surfaces at which the nanoparticles migrate along the blood flow.[108–110] This is significantly influenced by the size and geometry of the nanoparticle, and small, spherical particles tend to migrate at a considerable distance from endothelial surfaces, limiting both active and passive targeting strategies. When targeting tumors, another significant barrier is the high intratumoral pressure caused by interrupted vasculature, aggressive cellular growth, fibrosis, dense extracellular matrix, and impaired lymphatics.[111–115] For nanoparticles in general, cellular internalization and endosomal escape also present formidable barriers, with the size and surface decoration of nanoparticles affecting the route of internalization and intracellular fate.[116–118] Although the cellular uptake and intracellular trafficking to the site-of-action for SNAs is well demonstrated on various cell lines, the scavenger mediated endocytosis cannot be considered universally applicable for all cell types.

The formation of protein corona is an important factor on the biodistribution SNAs.[119] Specifically, the ability of proteins to adsorb onto SNAs result in their internalization by macrophage cells, leading to their accumulation in the liver and spleen after being administered intravenously typical for nanoparticles. Interestingly, the sequence of the ONs contributes to the macrophage internalization as G-rich SNAs attract a greater variety and number of proteins than poly-T SNAs resulting in enhanced macrophage cellular uptake *in vitro* and liver and spleen accumulation *in vivo* (Figure 5). Remarkably different biodistribution properties of SNAs bearing different ON sequences highlight the importance of sequence designing in therapeutic SNAs.

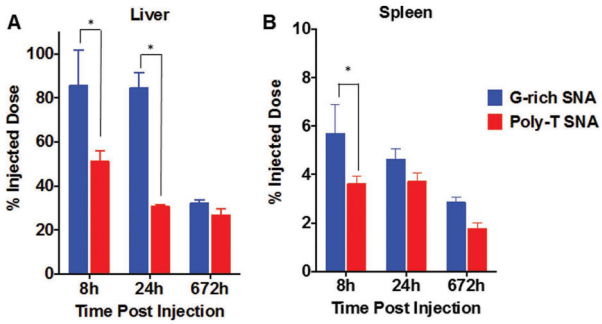

Figure 5. The effect of ON sequence to the organ accumulation of SNAs. Reprinted with permission from *Small*, 2017, 13 (16), 1603847.

SNAs have in general shown accumulation in liver and spleen after systemic administration. In addition, minor accumulation in lungs, kidneys, heart, brain, and intestines have been observed.[99,119–121] In additon, interesting biodistribution profiles have been obtained from studies with glioblastoma xenograft mouse model as gold nanoparticle based SNAs have been proven to cross both BBB and brain-tumor barrier to silence genetic lesions and reducing tumor burden.[120,122], with results translating to clinical progress[123]. In these studies, accumulation to tumor relied on passive targeting via enhanced permeability and retention (EPR) effect[111] and in healthy mice tissue distribution was primarily in the liver and spleen.[120] Despite the promising results, relying solely on passive accumulation via EPR is a controversial strategy as it is not universally translating to clinical efficacy against all tumor types.[124,125]

1.3 DNA dendrons

DNA dendrons are an interesting multivalent agents for intracellular delivery. They don´t have the full SNA architecture with spherical morphology, which might be beneficial in some applications as the high-valency three-dimensional full SNA structure has limited number of specific sites for the conjugation of other ligands. DNA dendrons can be synthesized by hybridization-based approach or covalently utilizing solid-phase oligonucleotide synthesis. The hybridization-based techniques rely on non-covalent interactions which make them vulnerable to dissociation in biological environments.[126,127] On the other hand, solid-phase DNA synthesis that utilizes phosphoramidite chemistry permits the construction of specific structures that are covalently linked.[128,129] However, branching the covalently elongating oligonucleotide chain typically decreases the yield.

Distler et al. took a systematic approach to improve the yield of covalent DNA dendrons with poly-T sequences utilizing automated phosphoramidite based coupling. Molecularly defined dendrons could be generated by straightforward chemical synthesis in 10% yield.[130] These DNA dendrons showed increased cellular uptake and plasma retention proportioned to the number of ON branches and compared to linear ON. To study the *in vivo* properties, fluorescently labelled DNA dendrons, bearing three (3 BD), six (6BD) or nine (9BD) ON branches (Figure 6A), and linear ON T20 were intravenously administered to female mice and fluorescence was measured from plasma samples at 0-240 min time points (Figure 6B). As expected for linear ONs, T20 was cleared form plasma in less than twenty minutes but branching of the oligonucleotide chain elongated the circulation time indicated by measurable fluorescence at even 240 min time point for 6BD and 9BD. Cellular uptake was studied on bone-marrow derived dendritic cells harvested from C57BL/6 mice. Cells were treated with 50 nM solution of fluorescently labelled T20 strands

or a 3BD, 6BD, or 9BD dendron for 1 h in serum-containing media, and the cellular uptake was assessed via flow cytometry. This experiment showed that, only 29% of dendritic cells take up the linear T20, and the uptake percentage significantly increases with an increase in DNA dendron valency, as approximately 60% of cells take up 3BD, and about 90% of cells take up 6BD and 9BD (Figure 6C). Measuring the median fluorescence intensity (MFI) from DNA-positive cells revealed that the valency has great effect on the amount of DNA taken up by the cells as an almost 20-fold increase in MFI was measured for cells treated with 6BD and 9BD compared with the T20 (Figure 6D). These *ex vivo* and *in vivo* findings show that full SNA architecture is not necessary for some of the beneficial biological properties associated with SNAs. In addition to delivery of the ON sequences, DNA dendrons can be used as agents for the delivery of biomolecular cargo. This was demonstrated by Distler and co-workers by conjugating ovalbumin 1 peptide to pyridyl disulphide-containing cross-linker in the stem ON via a disulphide exchange reaction. These peptide-DNA conjugates had similar internalization properties compared to unconjugated DNA dendrons.

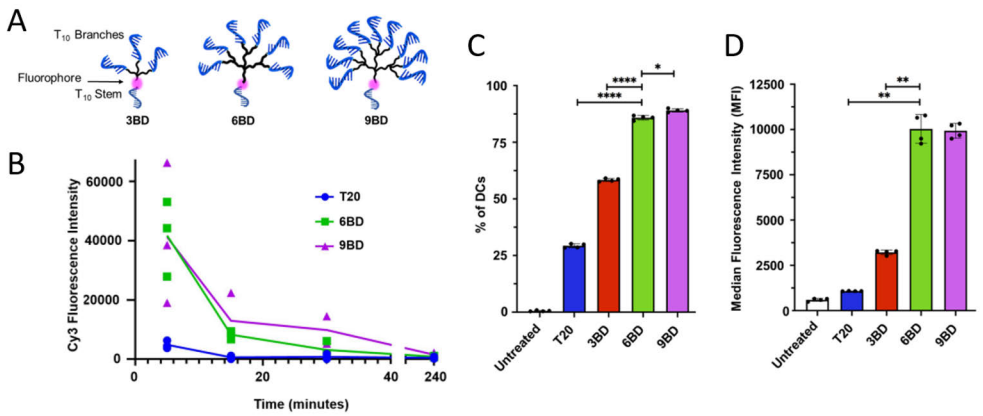

Figure 6. **A)** Structure of DNA-dendrons. **B)** Time-fluorescence profile measured from blood samples. **C)** Fraction of dendritic cells that have internalized DNA-particles (DNA-positive cells) among the dendritic cell (DC) population. **(D)** Median fluorescence intensities (MFIs) of DNA-positive cells. *, $p < 0.05$; **, $p < 0.01$; ****, $p < 0.0001$. Adaptated with permission from *J. Am. Chem. Soc.* 2021, 143 (34), 13513−13518.

1.4 Targeted delivery of oligonucleotides

The idea of targeted delivery of therapeutic modalities dates back in the early twentieth century when a German doctor, Nobel laureate Paul Ehrlich, introduced the magic bullet: an idea of the possibility to kill specific pathogens without harming

the body itself. This could be seen as the first conceptualization of targeted delivery, and from then on has intrigued scientists to look for targeted therapy solutions.[131]

Targeted delivery of therapeutic ONs has been achieved with various strategies by functionalizing the ONs with targeting moieties, such as antibodies, peptides, or small molecules, which can specifically recognize and bind to receptors or antigens on the surface of target cells. There are several advantages for targeted delivery of therapeutic oligonucleotides over systemic delivery. Targeted ONs can selectively accumulate in the desired tissues or cells, leading to higher local concentrations and increased therapeutic efficacy, minimizing the needed dosage. Furthermore, off-target effects and toxicity can be decreased, as the ONs are less likely to accumulate in non-target tissues.[1,5]

1.4.1 Antibody-oligonucleotide conjugates

Antibodies (Abs) are proteins that can selectively recognize and bind to specific antigens which could be for example receptors on surface of the cell. Combining the target recognition of Abs to specific disease modulation properties of ONs is a well rationalized and widely studied methodology with best candidates already reaching clinical trials.[132] Antibody-oligonucleotide conjugates (AOCs) have been developed against various cancer types including breast, prostate, colon, brain and lung cancer, as well as other indications such as virus infections, leukemia, and muscular diseases.[133]

AOCs can be produced by various methodologies (Figure 7). Most widely techniques can be divided to four classes: i) including ionic interaction[134], ii) affinity binding[135], iii) direct covalent conjugation[136] iii), and iv) hybridization-based loading[137]. In general conjugating ONs to proteins presents challenges such as heterogeneity, hydrophobicity, aggregation, and stability of the linker.[138] Especially with multiple ON payloads, the ON constituent contributes substantially to the overall molecular weight and electrostatic properties of the chimeric construct affecting the physical and chemical properties such as target recognition of the Ab. The negative charge of the ON constituent can also dominate the overall charge profile of the construct, making the analysis and characterization of an AOC more challenging.

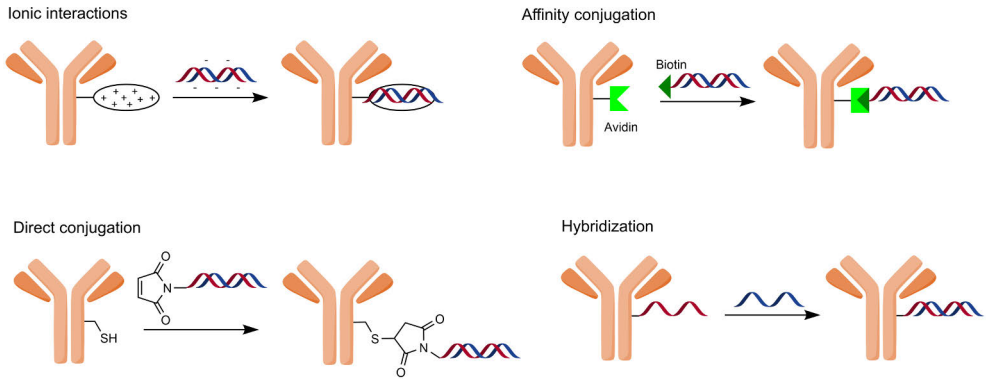

Figure 7. Methodologies for AOC preparation. Adapted with permission from *J. Clin. Med.* 2021, 10 (4), 838.

Zhang and co-workers have presented a hybridization-based methodology to produce Ab-SNA conjugates for cellular targeting (Figure 8).[139] In their approach, single strand DNA with complementary to the sequence on SNA, was covalently conjugated human epidermal growth factor receptor 2 (HER2) targeting Abs via amide coupling to Ab´s lysine residues. This Ab-DNA was then mixed with gold nanoparticle-based SNA bearing a HER2 mRNA targeting antisense sequence (antiHER2-SNA) and purified with centrifugal filtration to yield Ab-SNA with average 1.9 Ab-DNAs hybridized to each SNA. The conjugate was found to be internalized to ovarian cancer cells (SKOV-3) more rapidly compared to unconjugated SNA. HER2 knockdown effect of the conjugate was demonstrated by Western Blotting. Two negative control conjugates (off-target Ab-antiHER2-SNA or on-target-Ab-scramble-SNA) were used to demonstrate that the HER2 knockdown was specific.

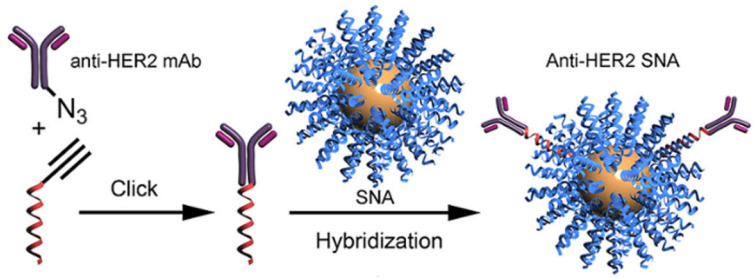

Figure 8. Hybridization based conjugation of SNA and Ab. Reprinted with permission from *J. Am. Chem. Soc.* 2012, 134 (40), 16488−16491.

1.4.2 Small molecule ligands

Small molecules selectively binding to specific receptors on the surface of cells can be conjugated to therapeutic oligonucleotides to target specific cells or tissues (Figure 9). They can be covalently introduced to ONs as modified building blocks in the solid-phase oligonucleotide synthesis (SPOS) or conjugated post-synthetically. Hybridization based introduction of small molecules can be achieved with a small molecule conjugated complementary strand.

N-Acetylgalactosamine (GalNAc) conjugation is a widely used strategy for hepatic delivery of therapeutic ONs.[140–144] GalNAc is a carbohydrate moiety that binds with high affinity to the asialoglyco-protein receptor 1 (ASGR1) expressed highly in the liver hepatocytes. First-in-class medication Givosiran, an antisense-based therapeutic bearing a triantennary GalNac structure for the treatment of acute hepatic porphyria[144], received it´s FDA approval in 2019.

Lipids, such as cholesterol or tocopherol, have been conjugated to ONs to enhance therapeutic potential. A tocopherol-siRNA conjugate has been reported to silence apolipoprotein B (apoB) related mRNA and induce phenotypic change in liver metabolism after systemic administration in mice.[145] Cholesterol siRNA conjugates have also shown ability to silence apoB[146], but they have also shown silencing of myostatin in murine skeletal muscle which is a promising result for the field of extrahepatic delivery of therapeutic ONs[147]. Simpler, long chain fatty acid conjugated siRNAs have also shown ability to downregulate apoB related mRNA adding more variety and chemistry options to this conjugate class.[148]

Folate, also known as folic acid, is a crucial member of the vitamin B family and essential nutrient playing significant role in the biosynthesis of purines and pyrimidines[149], as well as in amino acid metabolism[150]. Folate receptors are overexpressed in various cancers [151–155] making it a lucrative target for ON delivery. Dohmen et al. used folate conjugates to effectively deliver siRNA to KB/GFPLuc cells.[156] In this proof-of-concept study, internalization was confirmed by fluorescence microscopy, but no gene silencing activity was detected due to nonexistent endosomal escape. Adding polycationic carrier to the folate-siRNA conjugate facilitated the endosomal escape leading to dose-dependent silencing activity. This demonstrates how delivery of the therapeutic modality, in this case siRNA, is only part of the successful disease modulation.

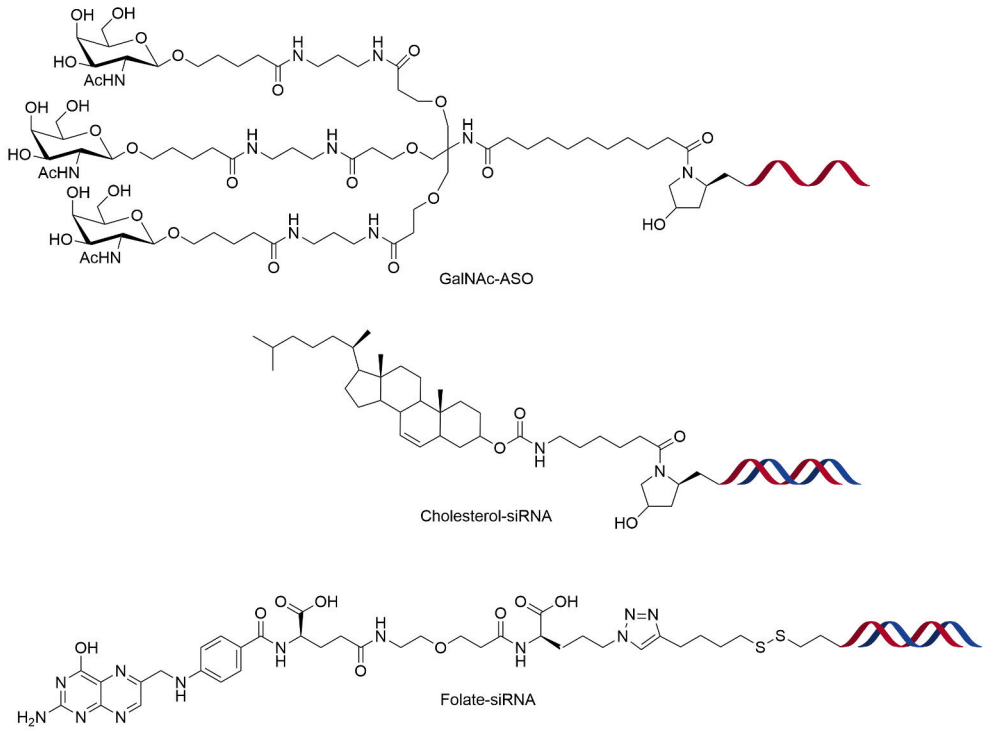

Figure 9. Small molecule-ON conjugates.[143,146,156]

Folate conjugation has been utilized also in tumor targeting of self-assembled RNA tetrahedrons, siRNA based nanoparticles consisting of over 200 base pairs (Figure 10A).[157] In *in vivo*, these RNA tetrahedrons accumulated primarily to tumor and kidney with minor accumulation to liver, spleen, lung and heart, after being injected to tail-vain of tumor bearing mice as monitored by fluorescence molecular tomography fused with computed tomography (FMT-CT). Compared to their parental siRNA, the RNA tetrahedrons reached the tumor more rapidly and had longer blood half-life (Figure 10B).

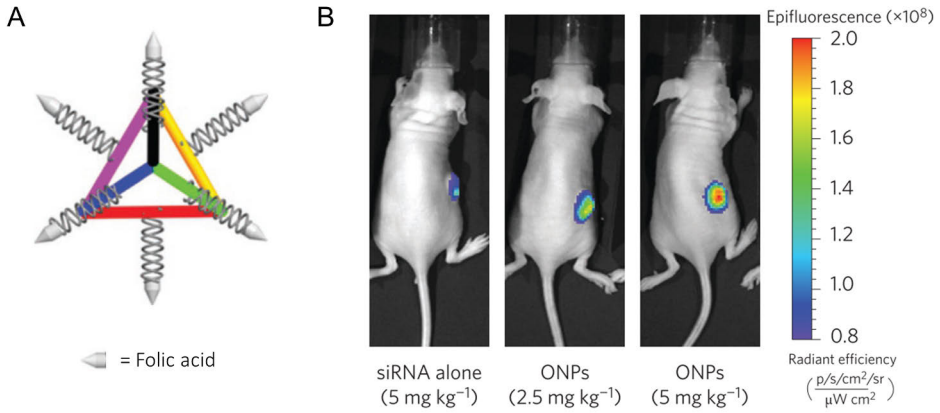

Figure 10. Folic acid targeting of RNA tetrahedrons. **A)** Structure of siRNA-folic acid conjugate. **B)** *In vivo* live fluorescence images showing dose-responsive accumulation of oligonucleotide nanoparticles (ONPs). Adaptated with permission from *Nat. Nanotechnol.* 2012, 7, 389-393.

1.4.3 Aptamers

Aptamers are short oligonucleotide sequences that can selectively bind to specific proteins or other molecules. They can be conjugated to therapeutic oligonucleotides aiming to targeted delivery to specific cells or tissues (Figure 11).[9] The conjugation can be carried out by an automated chemical synthesis as part of the elongating oligonucleotide chain or post-synthetically.[158] Aptamer siRNA chimeras have been successfully employed to targeted delivery and gene silencing of tumors expressing prostate-specific membrane antigen (PSMA).[159,160]

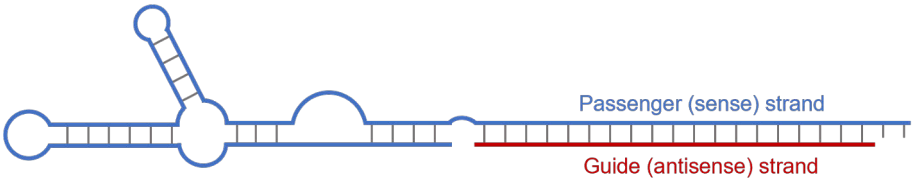

Figure 11. Aptamer-siRNA conjugate.[159]

Aptamer conjugation has been also applied to targeted delivery of SNAs. Xiao et al. hybridized a U87MG-cell specific aptamer to polystyrene-based SNA to enhance the delivery to tumor in a glioblastoma mice model.[121] Biodistribution after systemic administration was studied by second near infrared window (NIR-II) fluorescence imaging, and the aptamer conjugation was found to increase the delivery to tumor compared to non-targeted delivery. However, major accumulation was observed in liver and spleen, typical to nanoparticles.

1.4.4 Peptides

Peptides can selectively bind to specific receptors on the surface of cells and have been used for targeted delivery of therapeutic ONs in various applications (Figure 12). Peptide conjugation has been successfully used to facilitate targeted delivery of ASO payload to pancreatic beta cells[161] and angiotensin type 1 receptor (AGTR1) rich tissues heart, adrenal gland, and adipose relative to liver[162] after systemic administration. Conjugation to neurotensin has been used enhance potency of gapmer ASO to correct splicing of survival motor neuron pre-mRNA in the cortex and striatum after intracerebroventricular injection.[163] In addition to delivery to target tissue, peptide conjugation can be used also to enhance the cellular uptake of ONs. Cell-penetrating-peptides (CPPs) are short peptides which use energy-dependent or energy-independent mechanisms to pass through cell membranes facilitating the enhanced intracellular delivery of their cargo.[5,164] Various CPPs have been shown potential to increase significantly the delivery efficiency of nucleic acid cargoes.[165] Peptide conjugation have also been used in conjunction with charge neutral ON backbone chemistries.[166,167]

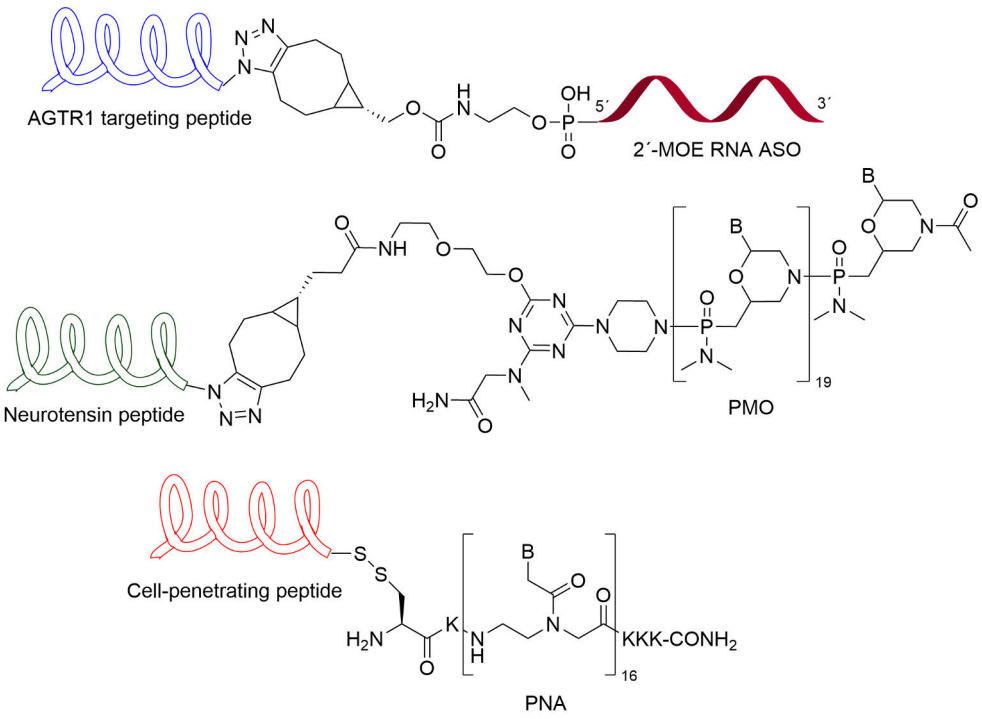

Figure 12. Peptide-ON conjugates.[162,163,167]

2 Aims of the Thesis

Therapeutic ONs are a versatile drug modality which can be used to modulate a variety of diseases beyond the scope of other modalities such as small molecules. However, their therapeutic potential is hindered by various recognized issues, such as rapid renal clearance, wide-spread biodistribution, and poor cellular uptake. SNAs solve some of the problems associated with ON therapeutics but targeted systemic delivery remains a significant hurdle. In general, conjugation of therapeutic molecules with cell type specific ligands has been used to enhance targeted delivery and cellular uptake.

This work aims to advance the field of therapeutic ON delivery. In this thesis, molecular spherical nucleic acids (MSNAs) are introduced as an alternative scaffold for therapeutic ONs. These molecularly defined structures allow specific attachment of reporter groups and targeting ligands while increasing the ON payload. Additionally, development of radiochemical labelling methodology allows accurate study of biodistribution properties of these molecular entities. Furthermore, bioconjugation to antibodies could enhance the targeted delivery of MSNAs.

Specifically, the aims of the thesis are as follows:

i) To develop an efficient method for site-specific Ab-ON conjugation utilizing SpyTag-SpyCather protein domain pair.

ii) To develop controlled synthesis and characterization of [60]fullerene-based MSNAs.

iii) To develop method for efficient introduction of radiolabel to MSNAs and study the biodistribution of MSNAs by positron emission tomography/computed tomography (PET/CT) imaging.

iv) To demonstrate applicability of MSNAs as an alternative covalent ON formulation for Ab-targeted delivery of ON therapeutics.

3 Results and Discussion

3.1 Site-specific AOCs via SpyTag-SpyCatcher system

3.1.1 Introduction

SpyCatcher/SpyTag is and efficient and site-specific protein ligation method which originates from *Streptococcus pyogenes* bacteria. In this methodology a SpyCatcher protein domain binds to a ligand peptide (SpyTag) forming an isopeptide bond between Asp and Lys residues of these peptide-protein complementarities.[168] This robust and fast reaction has attracted high interest in biotechnological research groups as it allows controlled preparation of novel protein-based biomaterials.[169] There are many reported potential therapeutic applications, but the immunogenicity of the bacteria originating Catcher-domain limits the therapeutic applicability.[170] However, this ligation is an excellent tool for diagnostic applications already in its current state.

In the first part of thesis, a SpyTag002-oligonucleotide conjugate was synthesized via SPAAC, and conjugated so single-chain variable fragment (scFv)-SpyCatcher fusion protein. The retained antigen binding properties of this scFv-ON construct were demonstrated, and it was exploited in immuno-PCR for the detection of small molecule analytes in low abundance.

3.1.2 Synthesis of the SpyTag002-Oligonucleotide conjugate and the generation of AOCs

3.1.2.1 Synthesis of SpyTag002-Oligonucleotide conjugate

A SpyTag002-oligonucleotide conjugate was synthesized for the preparation of AOCs which utilize the SpyTag-SpyCather protein domain pair. Azide modified SpyTag002 peptide (N_3-VPTIVMVDAYKPTK) and bicyclononyne (BCN) modified ON (BCN-5′-TTC ATC GCC CTT GCA AGC TTC GAC TAC CTA C-3′) were synthesized with corresponding automated synthesizers using commercial

building blocks and conventional coupling chemistries. The azide modified SpyTag002 peptide (1 equiv.) and a slight excess of the BCN-modified oligonucleotide (1.15 equiv.) were dissolved in water and they were allowed to react via SPAAC for 6h at 55˚C (Figure 13A). The reaction mixture was subjected to RP HPLC for purification (Figure 13B) and product fractions were lyophilized to dryness to obtain desired peptide-ON conjugate as white powder in 25% yield. The authenticity of the products was verified by MS (Figure 13C).

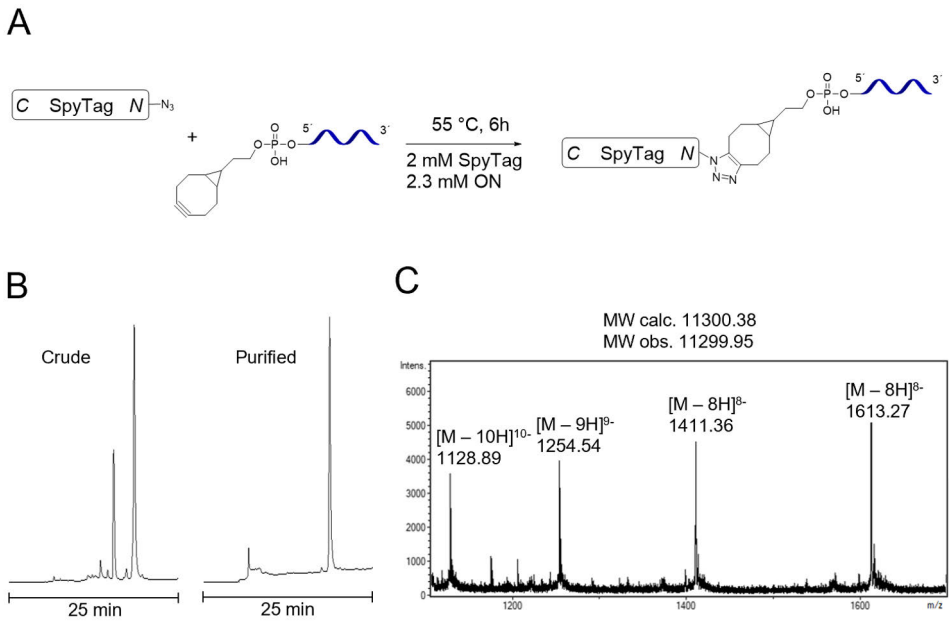

Figure 13. **A)** Synthesis of SpyTag002-oligonucleotide conjugate **B)** RP-HPLC profiles of crude and purified products **C)** MS (ESI-TOF) spectrum of purified product. Observed molecular mass is calculated from the most intense isotope combination at $[M - 7H]^{7-}$.

3.1.2.2 Conjugation of SpyTag002-Oligonucleotide to Cather proteins

The functionality of SpyTag002-ON in conjugation reaction with Catcher proteins was tested with two different SdyCatcher variants. SdyCatcher refers to a protein domain which originates from *S. dysgalactiae* bacteria, is homologous to original SpyCatcher domain and cross-reacts with SpyTag to form an isopeptide bond with equal efficiency as the original SpyCatcher protein. Both used SdyCatcher domains were site-specifically biotinylated and consisted of 83 aa with additional N-terminal His- and AviTag increasing the polypeptide length to 115 aa. The SdyCatcher 2 had two-point mutations compared to SdyCatcher 1 (K43E and I79L). SpyTag-10K

bearing 10 lysines in the *C*-terminus was used as a reference SpyTag species for the conjugation.

In the initial conjugation trials SpyTag002-ON or SpyTag-10K (0.2 nmol) and SdyCathcer 1 or SdyCatcher 2 (0.5 nmol) were incubated in 10 µl of phosphate-buffered saline (PBS) (pH 7.4) for 1 h at 37°C. Sodium Dodecyl Sulphate Polyacrylamide Gel Electrophoresis (SDS-PAGE) analysis was performed and both conjugation reactions with SpyTag002-ON were found to contain the desired product at ca. 25 kDa (Figure 14).

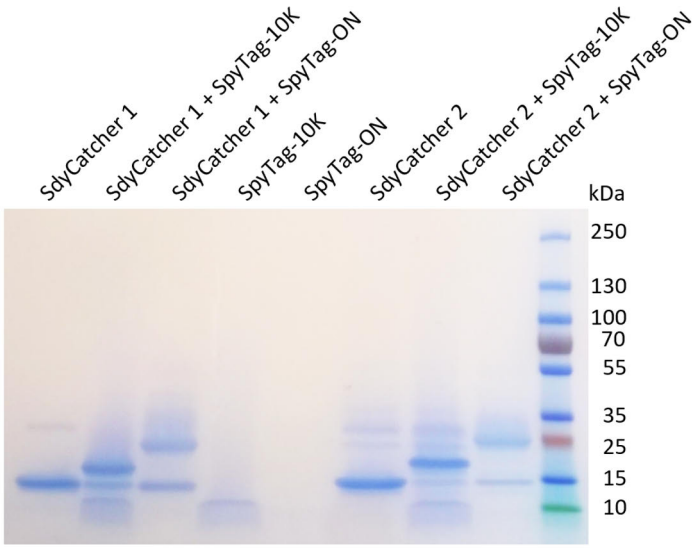

Figure 14. SDS-PAGE analysis of covalent isopeptide bond formation between SpyTag002-ON and SdyCatcher proteins 1 and 2.

Larger scale preparation of SdyCatcher-SpyTag-ON conjugate was performed in order to test purification protocol for final application consisting of sequential immobilized metal ion affinity and SEC steps. SdyCatcher 2 (12.8 nmol) and SpyTag002-ON (5.2 nmol) were incubated for 1 h at 37°C to allow isopeptide bond complex formation. Excess SpyTag002-ON was removed by affinity chromatography using nickel-nitrilotriacetic acid (Ni-NTA) agarose spin columns after which the eluate was subjected to SEC for further purification. In SEC, the desired product eluted as two peaks (Figure 15A, fractions 12-15) which both produced similar bands on SDS-PAGE at ca. 25 kDa indicating that on molecular level they are same protein construct (Figure 15B). First eluting peak probably represents a multimeric or aggregated structure and the second peak the monomeric protein. Product fractions were pooled to yield 2.7 nmol of desired conjugate (52% determined by UV-absorption at λ= 260 nm).

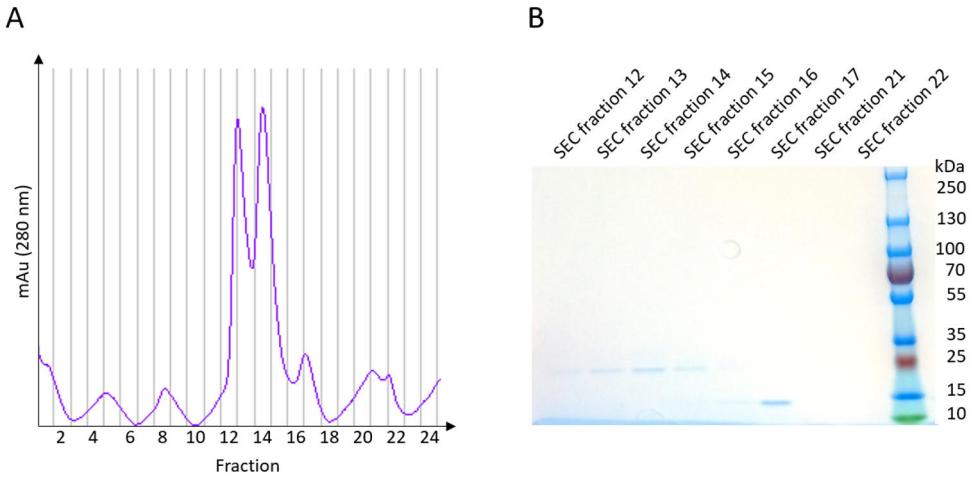

Figure 15. Purification of SdyCathcer-SpyTag002-ON conjugate **A)** SEC chromatogram of conjugation. **B)** SDS-PAGE analysis of SEC fractions.

3.1.3 Exploitation of SpyCatcher-SpyTag002-ON in immunoassays

Applicability of SpyCatcher-SpyTag002-ON constructs in immunoassays was evaluated at the Department of Biotechnology, University of Turku. Immuno-polymerase chain reaction (immuno-PCR) is an immunoassay in which the signal produced from antigen recognition is amplified with PCR to allow detection of analytes in low abundance. For this application, SpyTag002-ON was conjugated with single-chain variable fragment (scFv)-SpyCather fusion proteins to afford scFv-ON (scFv-SpyCather-SpyTag002-ON) conjugates. Their performance in immuno-PCR for microcystin-LR (MC-LR) and 17β-estradiol (E2) detection was evaluated (Figure 16). The assay allowed robust detection of MC-LR and E2 at lowest in 2 nM and 1 nM concentration, respectively. The overall effect of ON-conjugation to the antigen recognition properties of scFvs was studied by comparing the performance scFv and scFv-ON in time-resolved fluorescence immunoassay TRFIA. The compared constructs did not show major differences in binding demonstrating that construction of scFv-ON does not compromise the antigen recognition properties of scFvs. This is expected due to the fusion of SpyCatcher to the C-terminus of the scFv, distant from the antigen-binding site.

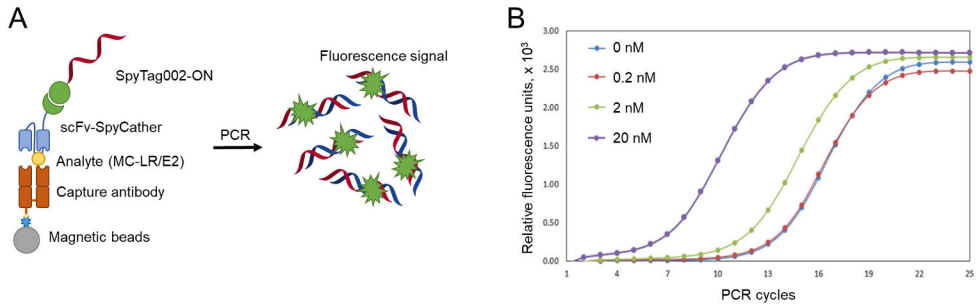

Figure 16. Exploitation of SpyCatcher-SpyTag002-ON in immuno-PCR. **A)** Schematic overview of immuno-PCR. **B)** Representative run profile vs. PCR cycles from microcystin-LR detection.

3.2 Synthesis of heteroantennary MSNAs

3.2.1 Introduction

Molecular spherical nucleic acids (MSNAs) are well-defined spherical formulation for the delivery of therapeutic ONs. They incorporate twelve ON arms which can bear two distinct functionalities (1 + 11) allowing utilization of e.g., tissue specific ligands and labelling group. By mono-labelling, the effect of the labelling group to the biophysical characteristics of MSNA can be minimized. The distinct arm can be also used for site-specific conjugation to targeting moieties as demonstrated in section 3.4.

In the second part of the thesis, controlled two-step SPAAC-based assembly of heteroantennary MSNAs is demonstrated with various ONs. Various analytical techniques are used for the characterization MSNAs.

3.2.2 Controlled synthesis of heteroantennary MSNAs

3.2.2.1 Azide functionalization of [60]fullerene

For the SPAAC based two-step assembly of MSNAs, [60]fullerene (C_{60}) was azide derivatized by exposing it to Bingel cyclopropanation with bis (2-(2-(2-(2-azidoethoxy)ethoxy)-ethoxy) malonate (Scheme 1). The reaction produces a tar-like crude mixture which must be purified with subsequent normal phase silica gel and RP HPLC purifications. Despite the extensive purification procedure, the overall yield for the desired 12-arm azide-derivatized core **1** was routinely 10-15%. The main side product of the reaction is an 11-arm derivative which hampers the assembly, purification, and identification of the target MSNAs. The homogeneity of

the 12-arm purified product can be verified by exposing it to SPAAC reaction with an excess of small molecular alkynes (e.g. bicyclo[6.1.0]non-4-yn-9-ylmethanol) and subjecting the reaction mixture to MS analysis.

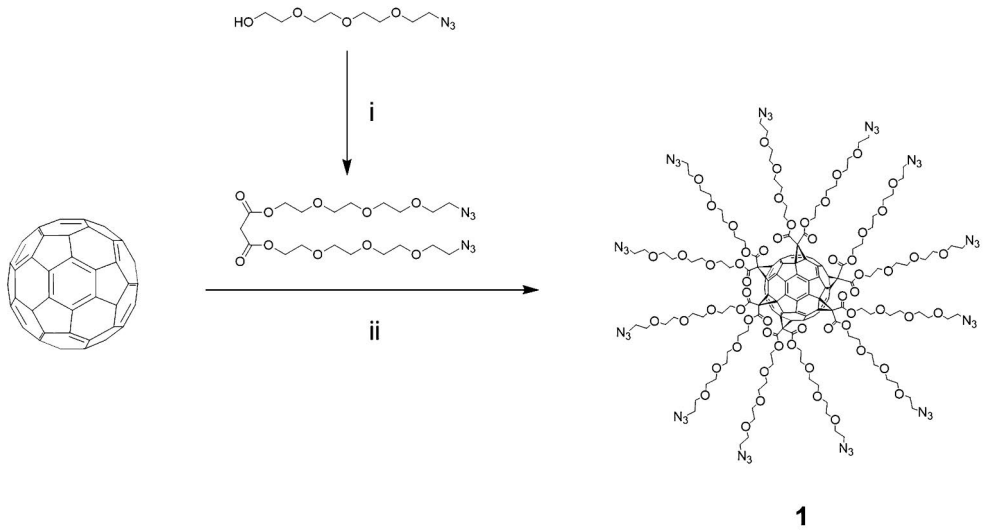

Scheme 1. Conditions i) Malonyl chloride, $NaHCO_3$, DCM, under nitrogen, 0°C to r.t. overnigth. ii) CBr_4, 1,8-diazabicyclo[5,4,0]undec-7-ene (DBU), o-dichlorobenzene under argon, 3 days at r.t.

3.2.2.2 Synthesis of oligonucleotides

For the SPAAC-based controlled assembly of heterofunctionalized MSNAs, a set of BCN-modified ONs (**ON1-ON10**) were synthesized on an automated DNA/RNA synthesizer using commercially available phosphoramidite building blocks and conventional synthesis conditions. The 3′-modified ONs, **ON8** and **ON10**, were synthesized using previously reported customized solid supports[171,172] with a 1,4,7,10-tetraazacyclododecane1,4,7,10-tetraacetic acid (DOTA) and a D-galactose moiety, respectively. **ON1-ON7** and **ON9-ON10** were cleaved from the solid support by overnight incubation in aq. ammonia at 55°C. A two-step cleavage protocol was used for the **ON8**: i) 0.1 mol L^{-1} aq. NaOH for 3 h at 55°C, followed by neutralization with 1.0 mol L^{-1} aq. NH_4Cl. ii) overnight incubation in concentrated aq. ammonia at 55°C. The ONs were purified by RP HPLC, their authenticity was verified by MS (ESI-TOF) spectroscopy and yield was determined by UV-absorbance at 260 nm. **ON1** and **ON2** are short model sequences which were used first to study the functionality of the two-step assembly of MSNAs. **ON3-ON10** are biologically active sequences. **ON3-ON5** contain a HER2 downregulating antisense sequence.[82] Phosphorothioate sequence on **ON6-ON7** is a splice switching ON that

downregulates expression of androgenic receptor variant (AR-V7) in prostate cancer cells.[173] The 2´-*O*-methyl modified sequence on **ON8-ON10** is complementary to microRNA 15b, involved in hepatocyte apoptosis.[174]

3.2.2.3 Two step SPAAC-based MSNA assembly

In a previously published protocol[82], azide modified C_{60}-core was treated with an excess of alkyne modified ONs (2-3 equiv. alkyne/azide) in aqueous 1.5 M NaCl solution. In our hands, this led to complicated mixture of products. The different solubility properties of the lipophilic C_{60}-core **1** and hydrophilic ONs retarded the reaction. Different reaction conditions regarding ON and core equivalents, DMSO/H_2O ratios and temperature were tested, which eventually led to our published two-step MSNA assembly protocol. Azide derivatized C_{60}-core **1** was first treated with a substoiciometric amount of BCN-ON **ON1-3**, **ON6** or **ON8** in DMSO at r.t. overnight (Scheme 2). The reaction mixture contained also <10% water from the ON stock solution. The excess of **1** varied from 3-5 equivalents, all producing acceptable results with the monosubstituted C_{60}-ON-conjugate as the main product. The reaction mixture was subjected as such to RP HPLC and the C_{60}-ON-conjugates **C1**-**C7** were isolated in 30-50% yield based on UV-absorbance at 260 nm. The crude product produced a comparable RP HPLC profile to the purified product (Figures 17A and 17B) indicating the overnight incubation led to consumption of BCN-ON. The authenticity of monosubstituted C_{60}-ON-conjugates **C1**-**C7** was confirmed by MS (ESI-TOF) (Figure 17C). C_{60}-ON-conjugates **C3** and **C6** were fluorescently labelled with Alexa Fluor 488 (AF488) label by treating them with an excess of AF488 NHS ester in aqueous borate buffer (pH 8.5) overnight in r.t. (Figures 17D and 17E) Fluorescently labelled conjugates **C4** and **C7** were isolated from labelling reagent by RP HPLC in 40-50% yield based on UV-absorbance at 498 nm and their authenticity was confirmed with MS (ESI-TOF). For the full decoration, **C1**-**C7** were treated with a slight excess (1.2 equiv. / azide arm) of BCN-ONs **ON1**, **ON5**, **ON6**, **ON9** and **ON10** in 1.5 M NaCl for three days. The mixtures were purified with RP HPLC to yield 12-arm **MSNA1-MSNA6** in 35-57% yield based on UV-absorbance at 260 nm (Figures 17F and 17G). For the AF488-labelled **MSNA3** and **MSNA4** yield was also determined by UV-absorbance at 488 nm, matching with that determined at 260 nm.

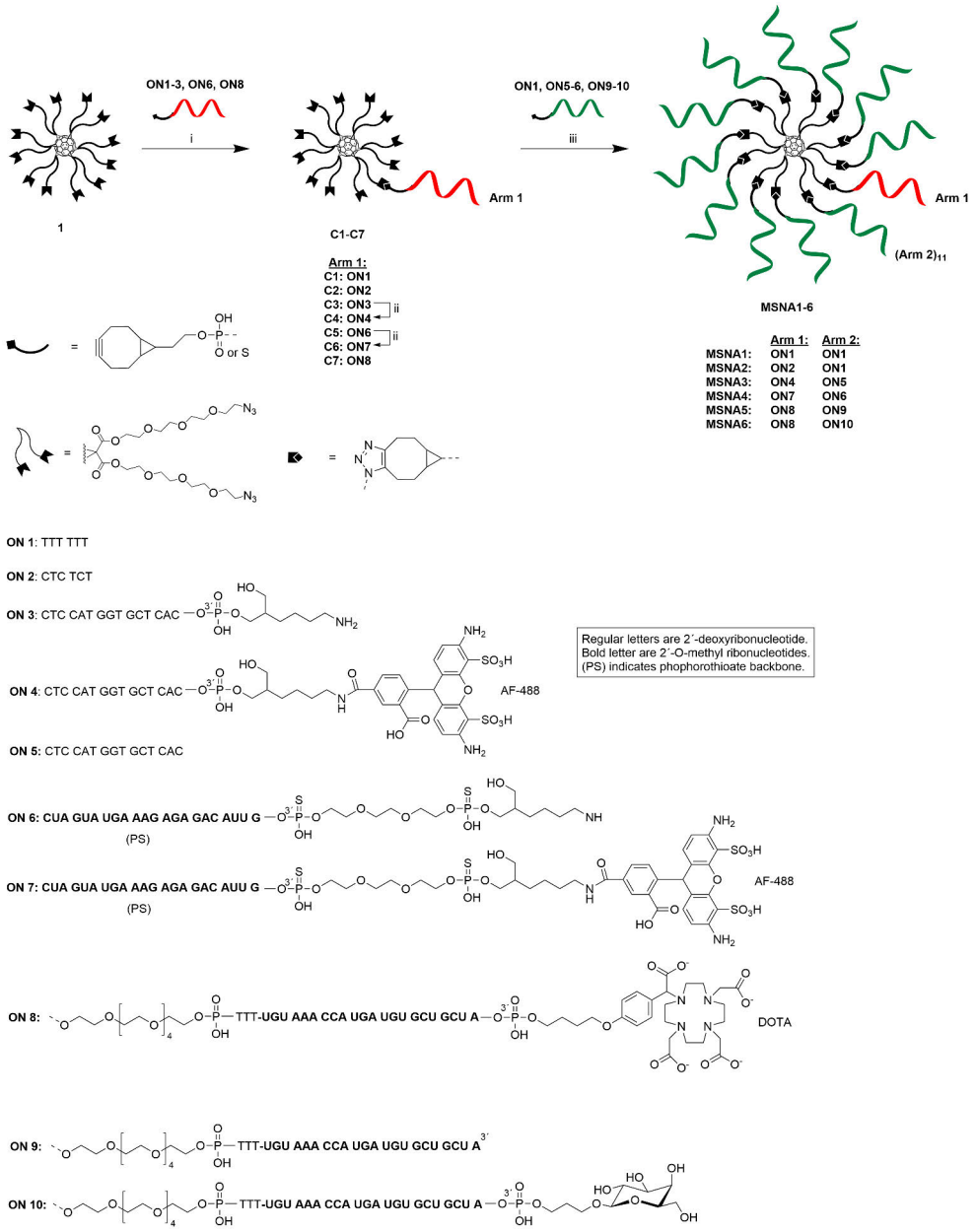

Scheme 2. Conditions: (i) BCN-modified oligonucleotide, **1** (3-5 equiv.) in DMSO, overnight r.t., (ii) AF-488 NHS ester, 0.1 M sodium borate (pH 8.5), overnight at r.t., (iii) **C1**−**C7**, BCN-modified oligonucleotide (1.2 equiv./arm) in aqueous 1.5 M NaCl, 3 days at r.t.

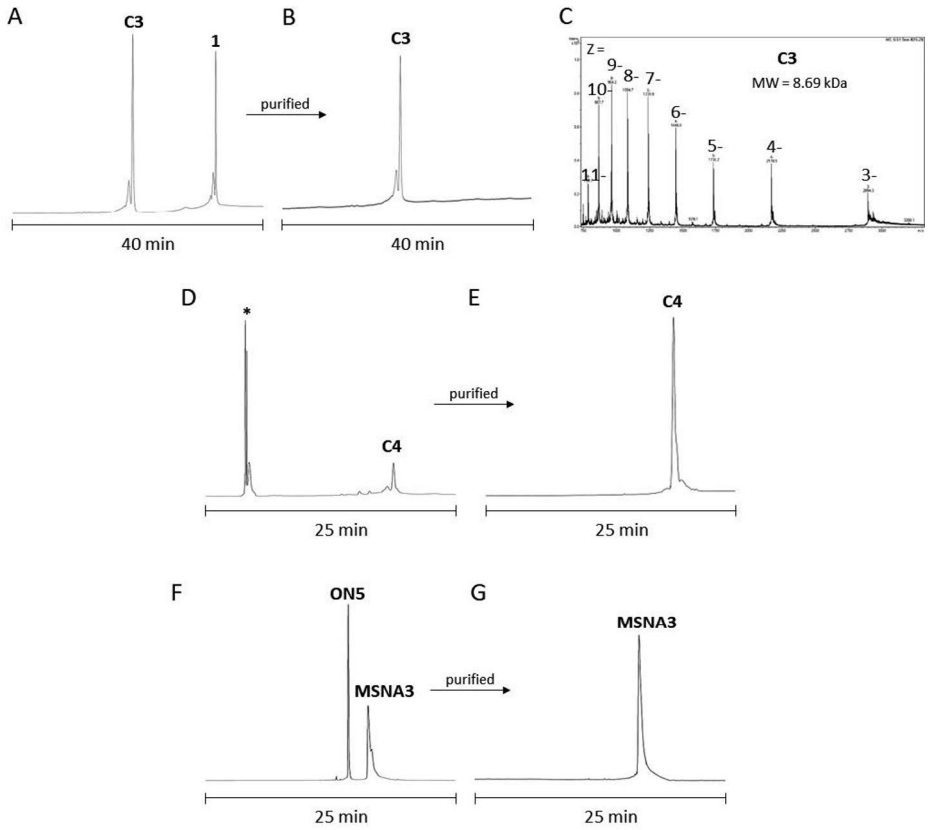

Figure 17. Example of RP-HPLC profiles and MS characterization from MSNA assembly. **A)** crude and **B)** purified product **C3**. **C)** MS spectrum of the monofunctionalized C_{60}-core **C3**. **D)** crude (* is from labeling reagent) and **E)** purified AF488-labelled product **C4**. **F)** crude and **G)** purified product **MSNA3**.

3.2.2.4 PAGE

Polyacrylamide gel electrophoresis (PAGE) was used to verify the homogeneity of **MSNA1-MSNA6** (Figure 18). MSNA samples (5 µL of 0.1 µM MSNA mixed with PBS) were mixed with 5 µl of TBE sample buffer and loaded onto a native 6% Tris base, boric acid, ehylenediaminetetraacetic acid (EDTA), and acrylamide gel (TBE), electrophorized, stained and imaged. DNA ladder (100-1000 bp) was used to make electrophoresis runs inter comparable.

A sharp single band was detected for **MSNA1-MSNA3**. **MSNA4** showed a broad band which might be caused by the stereoisomeric PS backbone. For **MSNA5** and **MSNA6** most of the material was in sharp main bands, but smaller bands were detected with longer migration distance indicating that the decoration was incomplete. This demonstrates the usability of PAGE to evaluate homogeneity of MSNAs, as species with different decoration degrees can be distinguished.

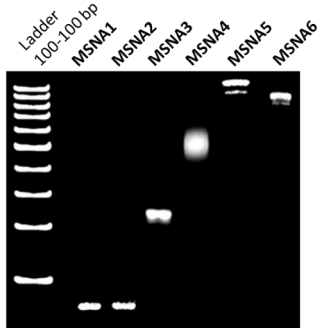

Figure 18. PAGE analysis of **MSNA1**-**MSNA6**.

3.2.2.5 Molecular weight determination with MS and SEC-MALS

A mass spectrometer equipped with a hybrid quadrupole orbitrap and nano electro spray ionization (ESI) was used to measure molecular weight of relatively small MSNAs (**MSNA 1** and **MSNA2**) (Table 1). Acceptable MS spectra were obtained. However, the obtained molecular masses were 0.1 and 0.2 kDa higher than the correct ones which may refer to formation of stable multiple sodium adducts. Size exclusion chromatography-multiple angle light scattering (SEC-MALS) can be used to estimate the homogeneity, aggregation tendency, and molecular weight of biomolecules, and is particularly useful for the characterization of large molecular weight compounds (>100 kDa) for which mass spectra is unobtainable. SEC-MALS was used for molecular weight determination of **MSNA3**-**MSNA6**. Samples (4 µl, 1 mg mL^{-1}) were eluted with 150 mM phosphate buffer (pH 7) through a 300 Å, 2.7 µm, 4.6 × 300 mm SEC column. Molecular weights determined by SEC-MALS corresponded relatively well with the calculated molecular weights (Table 1).

Table 1. Molecular masses of MSNA1-MSNA6.

MSNA	Calculated molecular mass (kDa)	Observed molecular mass (kDa)
MSNA1	27.6	27.8[a]
MSNA2	27.6	27.7[a]
MSNA3	61.2	62.6 ± 0.4[b]
MSNA4	107.3	106.8 ± 3.6[b]
MSNA5	109.9	109.3 ± 2.1[b]
MSNA6	113.2	107.4 ± 2.3[b]

[a] Hybrid quadrupole-orbitrap spectrometer with nano ESI-ionization. [b] SEC-MALS.

3.3 *trans*-cyclooctene modified MSNAs for study of *in vivo* biodistribution of MSNAs

3.3.1 Introduction

In the third part of the thesis, molecularly uniform [60]fullerene based MSNAs´ are synthesized and modified with *trans*-cyclooctene (TCO) to make them suitable precursors for biorthogonal inverse electron demand Diels-Alder reaction (iEDDA) based radiolabelling. Targeting ligand, folic acid, is introduced by hybridization-based strategy to enhance accumulation into folic acid receptor overexpressing tumor. Effect of the backbone chemistry (PO *vs.* PS), degree of radiolabelling and introduction of targeting ligand to the biodistribution properties are studied with PET/CT imaging.

3.3.2 Synthesis and characterization of MSNAs

3.3.2.1 Synthesis of *trans*-cyclooctene labelled MSNAs

General protocol for the synthesis of monofunctionalized MSNAs, described in more detail in section 3.2.2, was used for the preparation of TCO-modified MSNAs (Scheme 3.). In the first synthesis step core **1** (4 equiv.) was treated with **ON11**, **ON12** or **ON13** (1 equiv.) DMSO:water (9:1, *v*/*v*) and subjected to RP HPLC to yield monofunctionalized [60]fullerene-ON-conjugates **C8**-**10** in 45-55% yield. **C8**-**10** were treated with **ON14**, **ON15** or **ON13,** respectively, in aqueous 1.5 M NaCl. After RP HPLC purification, amino modified MSNAs **[NH_2]MSNA7-9** were obtained in 30-45% yield. The homogeneity of the **[NH_2]MSNA7-9** was confirmed by PAGE. TCO was introduced to **[NH_2]MSNA7-9** via amide coupling using TCO-PEG_4-NHS ester (100 equiv.) in aqueous 0.1 M sodium borate (pH 8.5). Excess TCO-PEG_4-NHS was removed by centrifugal filtration, and **[TCO]MSNA7-9** were obtained in 95% recovery. PAGE (Figure 20) and SEC-MALS (Table 2) were used to evaluate homogeneity and molecular weight of the MSNAs.

The active TCO-loading in [TCO]MSNAs might be substoichiometric due to two reasons: i) not all the amino-modified arms are substituted with TCO ii) TCO is prone to isomerization resulting in *cis*-cyclooctene (CCO) with significantly slower iEDDA reaction kinetics[175]. To use adequate amount of radiolabelling reagent, the active TCO-loadings in [TCO]MSNAs were determined with a model reaction with fluorescent label (6-methyl-tetrazine-carboxyfluorescein). The degree of labelling was determined by UV-Vis spectrometer (detection wavelengths and extinction coefficients: 260 nm, ε = 1 707 942 M^{-1} cm^{-1} for SNA and 492 nm, 83 000M^{-1} cm^{-1}

for label). For **[TCO]MSNA7** and **[TCO]MSNA8** TCO-content was ca. 25% and for **[TCO]MSNA9** 220%.

[TCO]MSNAs were radiolabelled at Turku PET Centre with fluorine-18 using 2-[^{18}F]fluoro-2-deoxy-*D*-glucose -labelled tetrazine (**[^{18}F]FDG-Tz**) and radiolabelled products **[^{18}F]MSNA7-9** were characterized by PAGE and SEC-MALS (Figure 20 and Table 2).

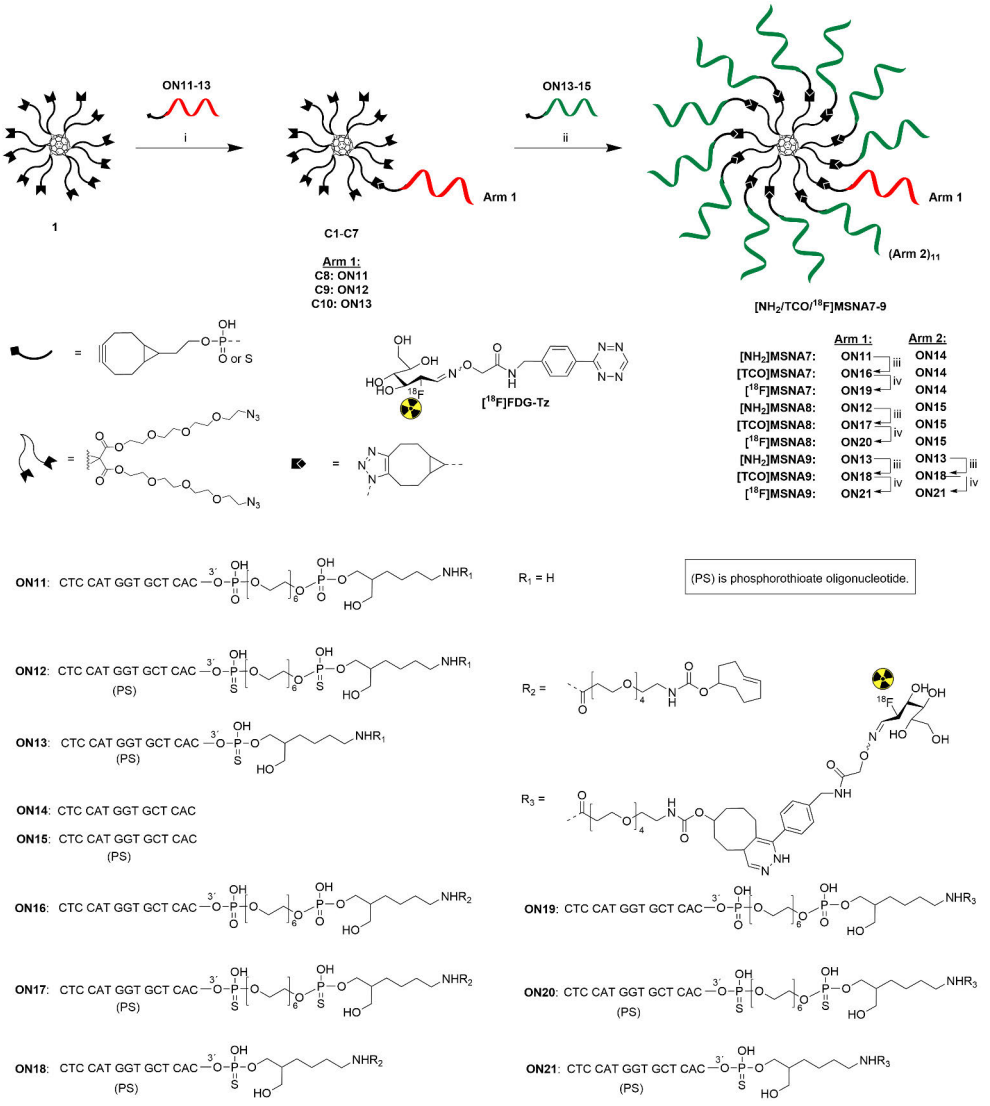

Scheme 3. Synthesis of radiolabeled MSNAs. (i) BCN-modified ON, C_{60}-core **1** (4 equiv.) in DMSO, overnight at r.t., (ii) **C8**, **C9** or **C10**, BCN-modified ON (1.2 equiv./arm) in aqueous 1.5 M NaCl, 3 days at r.t. (iii) TCO-PEG_4-NHS ester, 0.1 M sodium borate (pH 8.5), 4 h at r.t., (iv) [^{18}F]FDG-Tz in PBS (pH 7.4), 5 min at r.t.

3.3.2.2 Hybridization-based folate-decoration of MSNAs

A hybridization-based strategy was used to introduce folate decoration to PO **MSNA7** and PS **MSNA8** to enhance the accumulation of the MSNA to folate receptor rich tissues (Scheme 4). A folate conjugated complementary oligonucleotide **ON22** was synthesised by treating a 5´-amino modified ON with folic acid NHS ester for 16 h in room temperature, and then subjecting the reaction mixture to RP HPLC to yield the product (21%). The authenticity of **ON22** was confirmed with MS (ESI-TOF).

MSNA7 and **MSNA8** were treated with **ON22** (6-36 equiv.) in PBS for 1 h in r.t. and the hybridization was monitored by PAGE (Figure 19). The attachment of a folate-conjugated complementary strand through hybridization can result in a decreased electrophoretic mobility of MSNAs. In principle, using 12 or more equivalents of the complementary strand should produce comparable banding patterns on a gel, indicating complete hybridization of the MSNAs. For both **MSNA7** and **MSNA8,** equivalents of **ON22** over 12 didn´t decrease the migration distance on the gel. Interestingly, the hybridisation conjugates of **MSNA8** migrated further compared to those of **MSNA7**. However, no decrease in the migration distance was observed with over 12 equivalents of **ON22**. In conjunction with SEC-MALS analyses this confirmed that both **MSNA7** and **MSNA8** produce fully hybridized conjugates already with 12 equivalent treatments. For the biodistribution studies, the folate decorated PO **[TCO]MSNA10** and PS **[TCO]MSNA11** were synthesised by treating TCO-modified **MSNA7** and **MSNA8**, respectively, with 12 equivalents of **ON22** in PBS. **[TCO]MSNA10** and **[TCO]MSNA11** were radiolabelled at Turku PET Centre with fluorine-18 using **[^{18}F]FDG-Tz** and radiolabelled products **[^{18}F]MSNA10** and **[^{18}F]MSNA11** were characterized by PAGE and SEC-MALS (Figure 20 and Table 2)

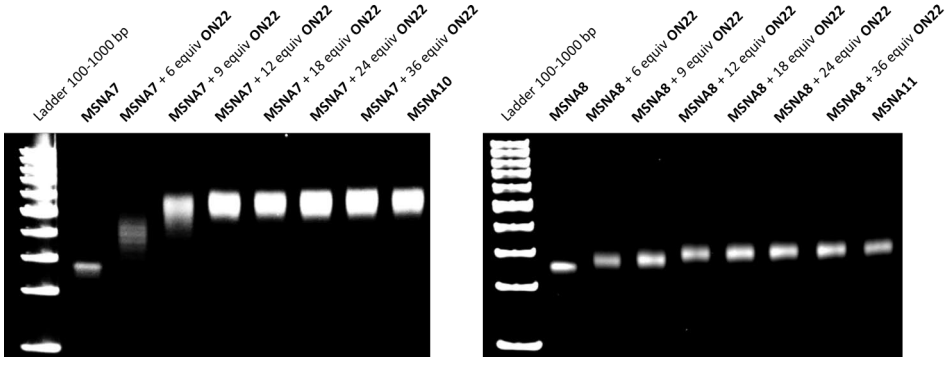

Figure 19. Hybridization based folate-decoration of **MSNA7-MSNA8** analyzed by PAGE. Folate-decorated **MSNA10-11,** used for radiolabeling, eloctrophorised for reference.

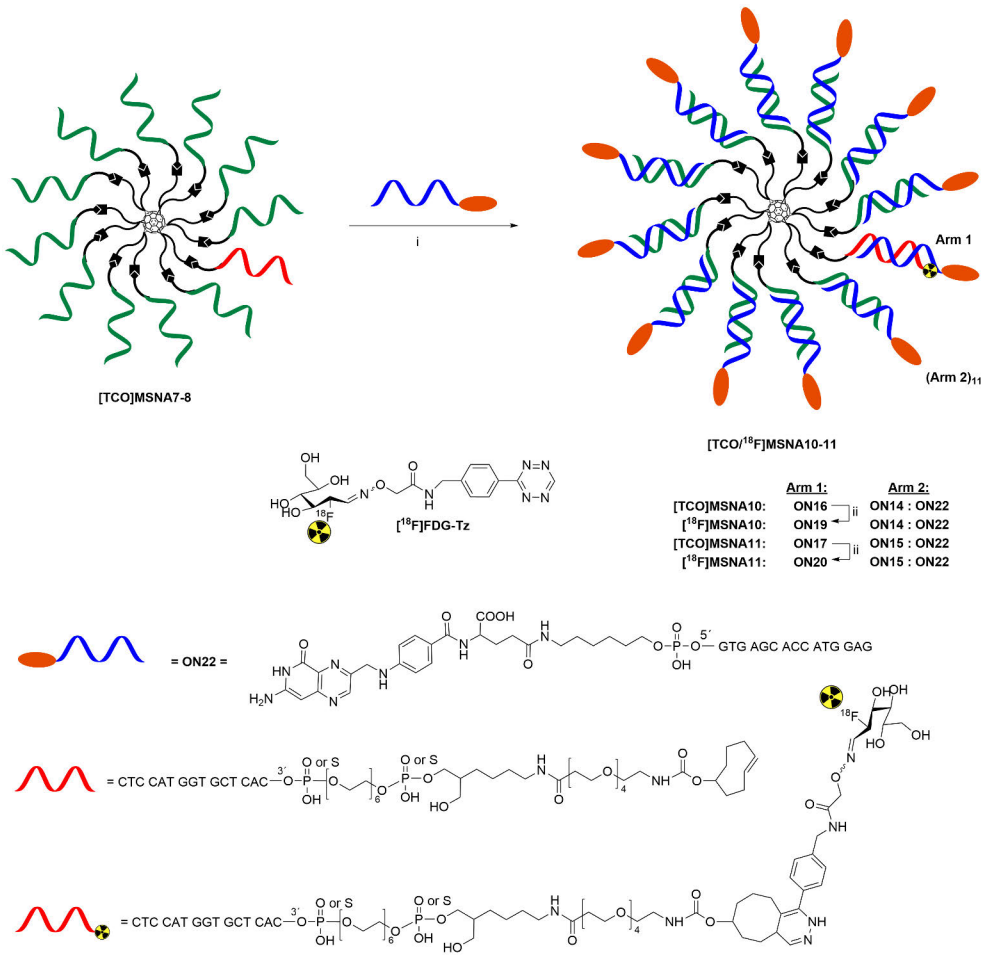

Scheme 4. Syhthesis of folate-decorated **[TCO/^{18}F]MSNA10-11**. (i) Folate-modified **ON22** in PBS, 1 h at r.t. (ii)**[18F]FDG-Tz** in PBS (pH 7.4), 5 min at r.t.

3.3.2.3 Characterization of MSNAs

PAGE was used to verify the homogeneity of **[NH$_2$/TCO/^{18}F]MSNA7-11** (Figure 20). MSNA samples (5 µL of 0.1 µM MSNA mixed with PBS) were mixed with 5 µl of TBE sample buffer and loaded onto a native 6% Tris base, boric acid, EDTA, and acrylamide (TBE) gel, electrophorized, stained and imaged. DNA ladder (100-1000 bp) was used to make electrophoresis runs intercomparable. MSNAs resulted in a single band.

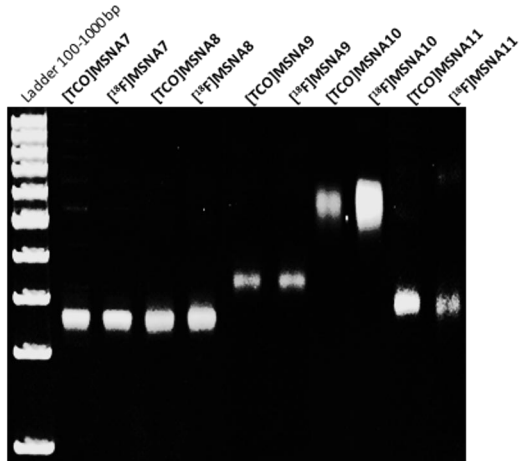

Figure 20. PAGE of **[TCO/^{18}F]MSNA7-11**.

SEC-MALS was used to evaluate the molecular weight of the **[TCO/^{18}F]MSNA7-11**. Samples (10-50 µL, 0.3-1 mg mL^{-1}) were eluted with 150 mM phosphate buffer (pH 7) through a 300 Å, 2.7 µm, 4.6 × 300 mm SEC column. Molecular weights determined by SEC-MALS corresponded relatively well with the calculated molecular weights (Table 2).

Table 2. Molecular masses of **[TCO/18F]MSNA7-[TCO/18F]MSNA11**.

MSNA	Calculated molecular mass (kDa)	Observed molecular mass (kDa)
[TCO]MSNA7	61.5	58.7 ± 0.2
[^{18}F]MSNA7	61.9	59.4 ± 0.3
[TCO]MSNA8	64.5	66.8 ± 0.5
[^{18}F]MSNA8	64.9	69.6 ± 0.1
[TCO]MSNA9	71.1	71.5 ± 0.2
[^{18}F]MSNA9	75.8	89.6 ± 0.2
[TCO]MSNA10	124.1	114.9 ± 0.1
[^{18}F]MSNA10	124.5	113.8 ± 0.1
[TCO]MSNA11	126.9	124.9 ± 0.1
[^{18}F]MSNA11	127.3	139.1 ± 02.3

The results from PAGE and SEC-MALS experiments, indicate that the described iEDDA based methodology is well-suited for radiolabelling of MSNAs, and that the homogeneity or structural integrity is not compromised in radiolabelling.

3.3.3 Biological evaluation

MSNAs were biologically evaluated in Turku PET Centre using *in vivo* PET imaging (Figure 21), *ex vivo* biodistribution and autoradiography. **[^{18}F]MSNA7-11** were administrated via tail vain into HCC1954 tumor-bearing mice and imaged by PET/CT for 60 min. A 15mer single strand PS oligonucleotide (**[^{18}F]ssDNA**) and **[^{18}F]FDG-Tz** were traced as comparison. **[^{18}F]MSNA11** showed increased circulation time compared to their PO MSNA analogues which might be due to improved enzymatic stability[90,176] and increased plasma protein binding[7,68,70]. PO **[^{18}F]MSNA7** was cleared rapidly likely due to degradation of PO backbone *in vivo* as protection towards nucleases might need higher density of ONs on the SNAs.[82,90] Compared to other PS MSNAs, **[^{18}F]MSNA9** with high TCO-content exhibited the highest liver accumulation leading to reduced fraction of particle reaching other tissues. PS **[^{18}F]MSNA8** showed liver accumulation like **[^{18}F]ssDNA**, and this was notably lower compared to that of typical nanoparticles.[93,120,122,177] Tumor accumulation was highest for folate decorated PS **[^{18}F]MSNA11** but this didn´t result in increased tumor/muscle ratio.

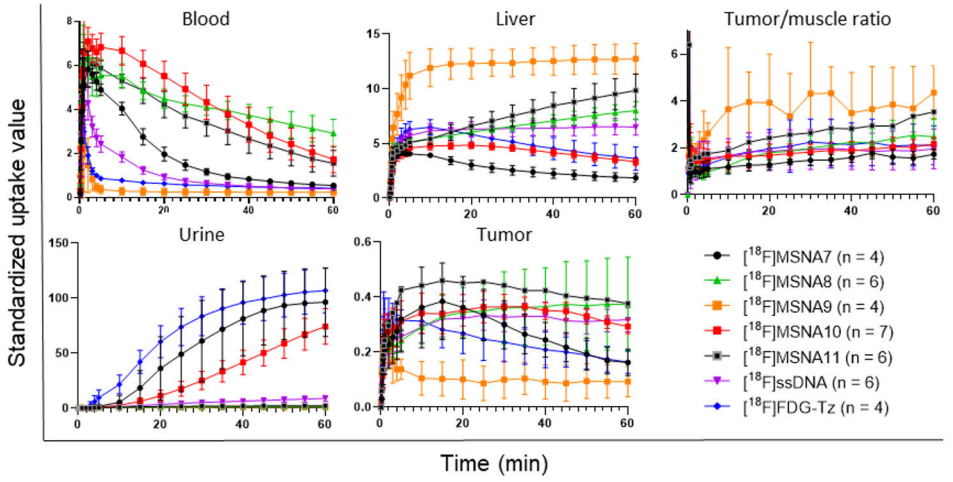

Figure 21. *In vivo* biodistribution of **[^{18}F]MSNA7-11**, **[^{18}F]ssDNA** and **[^{18}F]FDG-Tz**, in HCC1954 tumor-bearing female mice. Time-activity curves for blood, liver, tumor/muscle ratio, urine, and tumor.

3.4 Ab-MSNA conjugates for cellular targeting of ON therapeutics

3.4.1 Introduction

Ab-ON conjugates are therapeutically potent large chimeric bioconjugates which combine characteristic properties of individual parts; antibody acts as a target recognizing element where oligonucleotide serves as therapeutic agent or reporter group. During recent years the development of therapeutic AOCs have accelerated, and several molecules have entered the clinical trials[132]. ON payload can be increased by using SNAs as the oligonucleotide bearing unit[139]. Previously, hybridization-based conjugation of polydisperse gold nanoparticle-based SNA and Ab have been reported.

The fourth part of the thesis describes the applicability of hybridization-based approach and covalent conjugation of MSNAs and Abs. TCO-modified MSNAs presented in section 3.3.2.1 are suitable for conjugation with tetrazine modified Abs via biocompatible iEDDA reaction. This synthesis strategy can be utilized to obtain MSNA suitable for site specific covalent conjugation to glycan engineered tetrazine functionalized Ab. The functionality of covalent Ab-MSNAs for cellular targeted delivery, and anti-proliferation effects on cancer cells is demonstrated by *in vitro* methodologies.

3.4.2 Hybridization based Ab-MSNA conjugates

3.4.2.1 Synthesis of Ab-ON conjugate for hybridization with MSNA

For the hybridization-based Ab-MSNA(antisense) conjugation, a 5′-dibenzocyclooctyne (DBCO) modified ON(sense) was synthesised and conjugated to an antibody with SPAAC reaction. The 5′-DBCO modified oligonucleotide (DBCO-TEG-5′-GTG AGC ACC ATG GAG-3′) was synthesized on a 2.0 µmol scale by using an automated DNA/RNA synthesizer. Dibenzo-cyclooctyne was coupled as the last building block using a commercial phosphoramidite derivative bearing a tetraethylene glycol spacer. The crude ON was purified by RP HPLC. Isolated yield (32%) was determined by UV absorbance at 260 nm. The authenticity of the oligonucleotide was verified by MS (ESI-TOF).

Glycans on the heavy chains of IgG type antibody were azide-modified with commercial GlyCLICK technology which utilizes two enzymatic reactions. First the glycan chain is deglycosidated from the inner most *N*-acetylglucosamine (GlcNAc) by a specific endoglycosidase. Secondly, galactosyltransferase is used to attach uridine diphosphate N-azidoacetylgalactosamine (UDP-GalNAz) to the exposed

GlcNAc-residue yielding the site-specifically azide-modified Ab-N_3 (two azides / Ab).

DBCO-ON (10 equiv.) and Ab-N_3 (1 equiv.) were incubated overnight in room temperature in PBS after which the reaction mixture was subjected to SEC for purification. In SEC (Figure 22A), two major peaks were visible: one on the typical retention time of immunoglobulin G (IgG) antibodies (14 min) and one with longer retention time (19 min), probably corresponding the excess DBCO-ON. This indicated that the desired Ab-ON conjugate and unmodified antibody, if still present in the mixture, could not be separated. The antibody representing fractions at 14 min were collected, and their SDS-PAGE analysis showed the desired ON-conjugated heavy chain at ca. 55 kDa with no significant amount of unmodified heavy chain (Figure 22B).

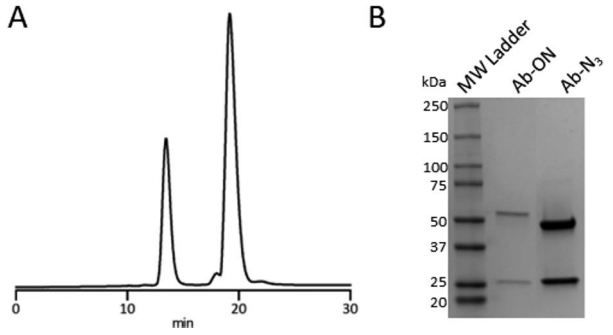

Figure 22. A) SEC profile of Ab-ON conjugation reaction **B)** SDS-PAGE analysis of Ab-ON conjugate.

3.4.2.2 Hybridization based conjugation of MSNAs to Abs

Fluorescently labelled HER2antisense **MSNA3** (from Scheme 2) was used as the MSNA constituent in the hybridization based conjugation trials. Ab-ON(sense) has two singlestrand ONs available as site of hybrisization based conjugation and the MSNA(antisense) has twelve sites of conjugation. Therefore a mixture of conjugate species is expected when mixing the Ab and MSNA. To study this conjugation behaviour, different ratios (5:1 - 1:5) of Ab and MSNA were mixed in micromolar concentrations in PBS and incubated overnight in room temperature (Scheme 5). Samples of reaction mixtures were electophorized in native conditions and the polyacrylamide gels were stained with Coomassie stain. Gels were imaged before and after staining (Figure 23). On native PAGE, the shape of the electrophorized species effect the migration so no direct size evaluation can be done based on the molecular weight ladder. In UV imaging before staining, constructs with MSNA constituent with Alexa-label are visualized. With higher Ab equivalents the amount of free MSNA is reduced and with 4-5 equiv. no free MSNA is observed on UV

imaging. With 5-2 equiv. of Ab, material is also visible in the bottom of the loading wells indicating formation of large complexes. On Vis-image after staining, no free Ab is present in any of the reactions. When comparing UV and Vis imaging, several bands can be visualized on both methods indicating formation of several conjugate species. Two of these conjugates migrated further than free Ab, which is interesting since larger conjugate species should migrate less. In these cases, the conjugate might have more MSNA, and the negative charge of ONs might enhance the mobility towards the cathode. Overall, these experiments demonstrate that hybridization-based conjugation is a viable strategy for the conjugation of MSNAs and Abs. However, this methodology as such gives poor control over the conjugation ratio and produces uncharacterizable mixture of products due to the infinite possibility for different conjugate species. The specificity of the conjugation could be enhanced by utilizing a strand with a different sequence compared to other strands coupled to the fullerene. This way there would be only one conjugation site in the MSNA.

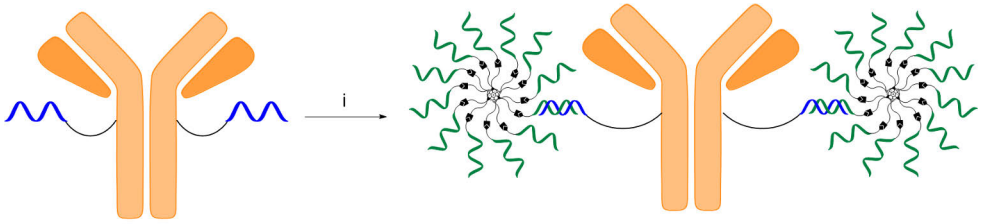

Scheme 5. Synthesis of hybridization-based Ab-MSNA conjugates. Conditions: (i) **MSNA3** (0.2-5 equiv.) in PBS for 16h in r.t. Note: The hybridization produces a mixture of products, and only one product specie is presented in the scheme.

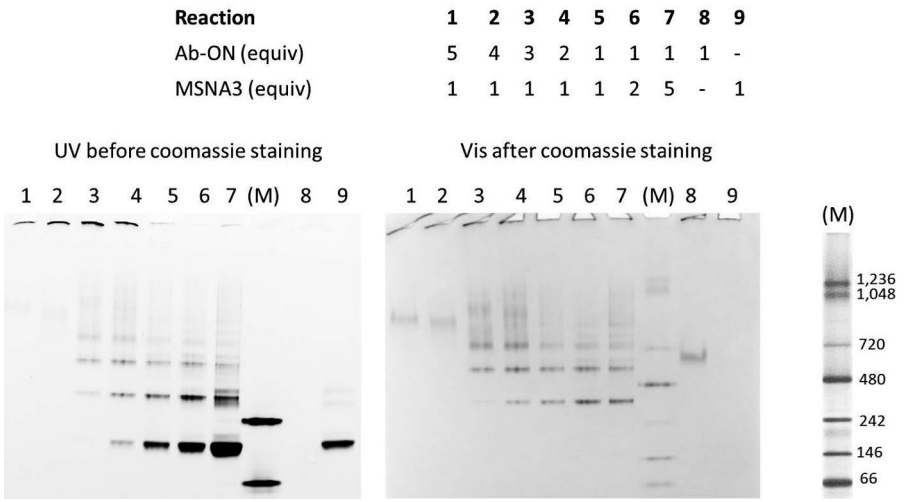

Figure 23. Native PAGE analysis of hybridization reactions between MSNA and Ab-ON. MSNA is visualized on UV and Ab on Vis. (M) molecular weight ladder.

3.4.3 Synthesis of covalent Ab-MSNA conjugates

3.4.3.1 Synthesis of TCO-modified MSNAs

The general protocol for the synthesis of monofunctionalized MSNAs presented in section 3.3.2.1 was used for the preparation of TCO-MSNAs, used for iEDDA-based conjugation with antibodies. In the first synthesis step, C_{60}-core **1** (4 equiv.) was treated with HER2antisense **ON11** or scramble **ON23** (1 equiv.) in DMSO:water (9:1, *v*/*v*) and subjected to RP HPLC to yield monofunctionalized [60]fullerenes **C10** and **C11** in 45-50% isolated yield (Scheme 6). **C8** and **C11** then were treated with HER2antisense **ON14**, scramble **ON24** or Cyanine5-labelled HER2antisense **ON26** in aqueous 1.5 M NaCl. After RP HPLC purification, amino modified MSNAs HER2antisense **[NH$_2$]MSNA7**, scramble **[NH$_2$]MSNA12** and Cyanine5-labelled HER2antisense **[NH$_2$]MSNA13** were obtained in 40-50% yield. The homogeneity of the [NH$_2$]MSNAs was confirmed by PAGE. TCO was introduced to [NH$_2$]MSNAs via amide coupling using TCO-PEG$_4$-NHS ester (100 equiv.) in aqueous 0.1 M sodium borate (pH 8.5). The excess TCO-PEG$_4$-NHS was removed by centrifugal filtration, and **[TCO]MSNA7**, **[TCO]MSNA12** and **[TCO]MSNA13** were obtained in 95% recovery. PAGE and SEC-MALS were used to evaluate homogeneity and molecular weight of the MSNAs.

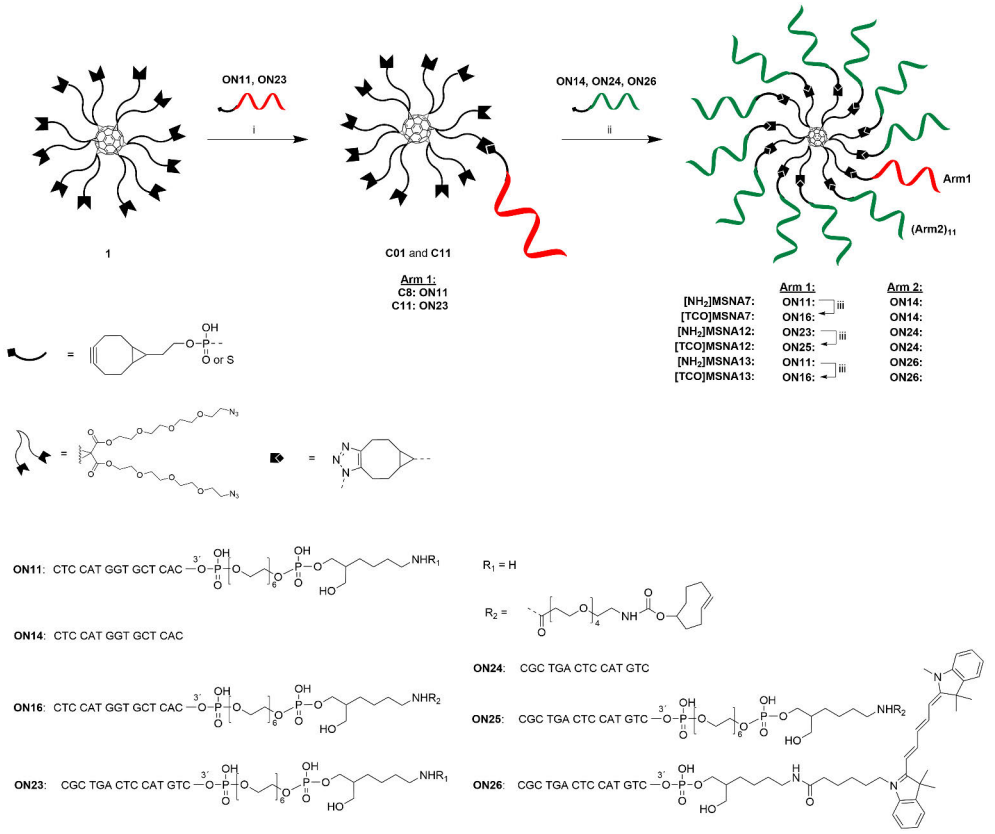

Scheme 6. Synthesis of TCO-modified MSNAs for conjugation with antibodies. (i) BCN-modified oligonucleotide, C_{60} core **1** (4 equiv.) in DMSO, overnight at r.t., (ii) **C8** or **C11**, BCN-modified (1.2 equiv./arm) in aqueous 1.5 M NaCl, 3 days at r.t., (iii) TCO-PEG_4-NHS ester, 0.1 M sodium borate (pH 8.5), 4 h at r.t.

3.4.3.2 Characterization of MSNAs

PAGE was used to verify the homogeneity of **[NH_2/TCO]MSNA7**, **[NH_2/TCO]MSNA12** and **[NH_2/TCO]MSNA13** (Figure 24). MSNA samples (5 µL of 0.1 µM MSNA mixed with PBS) were mixed with 5 µl of TBE sample buffer and loaded onto a native 6% Tris base, boric acid, EDTA, and acrylamide (TBE) gel, electrophorized, stained and imaged. DNA ladder (100-1000 bp) was used to make electrophoresis runs interoperable. MSNAs resulted in a sharp single band. Interestingly **[NH_2/TCO]MSNA13** migrated less than **[NH_2/TCO]MSNA7** and **[NH_2/TCO]MSNA12** which is due to the labelling groups.

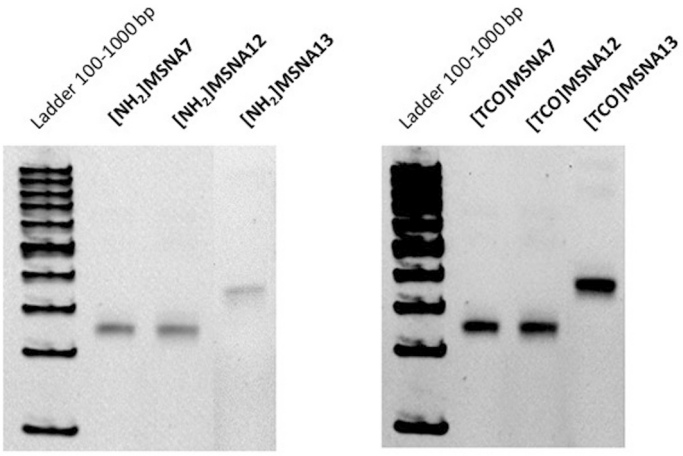

Figure 24. PAGE of **[NH2/TCO/]MSNA7**, **[NH2/TCO/]MSNA12** and **[NH2/TCO/]MSNA13**.

SEC-MALS was used to evaluate the molecular weight of the **[TCO/]MSNA7**, **[TCO/]MSNA12** and **[TCO/]MSNA13**. Samples (10 µl, 1 mg mL^{-1}) were eluted with 150 mM phosphate buffer (pH 7) through a 300 Å, 2.7 µm, 4.6 × 300 mm SEC column. Molecular weights determined by SEC-MALS corresponded relatively well with the calculated molecular weights (Table 3).

Table 3. Molecular masses of **[TCO/]MSNA7**, **[TCO/]MSNA12** and **[TCO/]MSNA13**.

MSNA	Calculated molecular mass (kDa)	Observed molecular mass (kDa)
[TCO]MSNA7	61.5	59.6±0.9
[TCO]MSNA12	61.5	59.2±0.9
[TCO]MSNA13	70.2	78.1±0.6

3.4.3.3 Tetrazine modification of antibodies

Glycans on the heavy chains of Trastuzumab (**Tra**) and isotype control **IgG** were azide-modified with commercial GlyCLICK technology, which is described in more detail in section 3.4.2.1. Azide-modified antibodies **Tra-N_3** and **IgG-N_3** were then treated with an excess (100 equiv.) of bifunctional sulfo-6-methyl-tetrazine-dibenzyl cyclooctyne (**Tz-DBCO**) for 4 h in room temperature and purified with spin column filtration to yield tetrazine modified antibodies **Tra-Tz** and **IgG-Tz** (Scheme 7i).

3.4.3.4 Conjugation trials with high TCO-load MSNA

Higher TCO-content **[TCO]MSNA9** is an interesting molecule to be used for the conjugation with Abs via iEDDA-based bioconjugation. The remained unreacted TCO-moieties on the MSNA may be used for iEDDA based radiolabelling. There is a chance for unfavourable oligo/polymerization, but this may be prevented by controlling the stoichiometry of the starting materials: Ab and MSNA. To test this hypothesis, **[TCO]MSNA9** (1-4 equiv.) was incubated with tetrazine modified **Tz-Tra** (1 equiv.) in micromolar concentrations for 4 h in room temperature. SDS-PAGE analysis revealed that all reactions contained both unmodified (50 kDa) and the desired MSNA-conjugated (ca. 110 kDa) heavy chains (Figure 25). Furthermore, larger molecular mass species above 250 kDa were present indicating formation of oligomeric complexes of Ab-MSNAs. These preliminary results were found to be discouraging to further study with high load **[TCO]MSNA9** and tetrazine-modified Abs. In the light of these results, mono TCO-loaded MSNAs should be used in iEDDA based Ab-conjugation to obtain a controlled mixture of products.

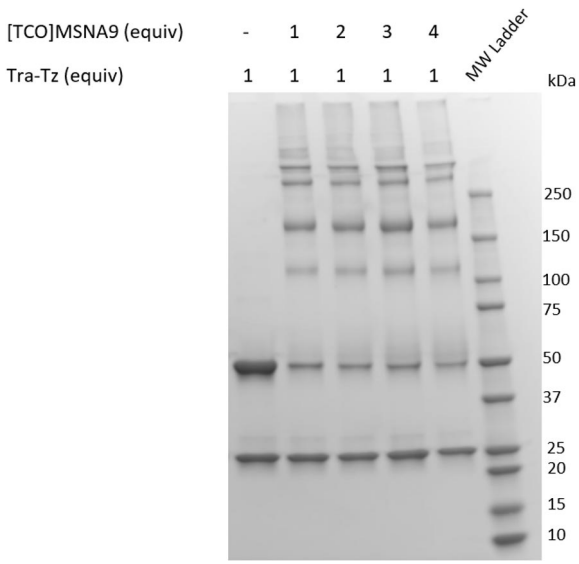

Figure 25. Conjugation of **Tz-Tra** and high TCO-loading **[TCO]MSNA9**.

3.4.3.5 Preparation of uniform Ab-MSNA conjugates

Tz-Abs have two reactive sites, therefore two-fold molar excess of mono TCO-labelled MSNAs would in theory mean 1:1 ratio of reactive TCO/Tz-species. However, our previous results suggest that the TCO derivatization of MSNAs with the before-described method is not quantitative (section 3.3.2.1). Considering these

results, conjugations of mono-TCO MSNAs to Abs was tested with different ratios of reactive species in micromolar concentrations (Scheme 7).

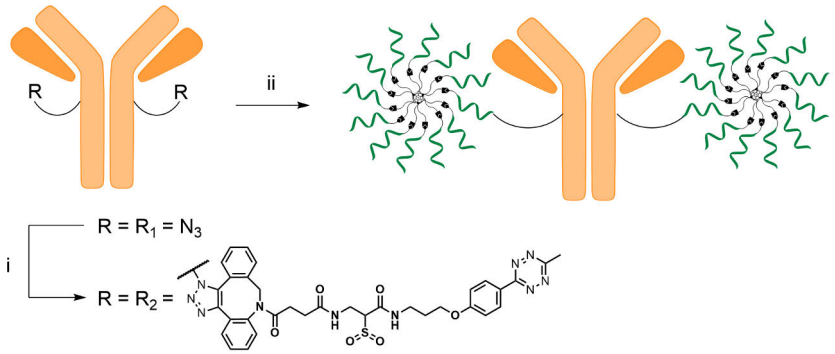

Scheme 7. Synthesis of covalent MSNA-Ab conjugates. Conditions: (i) N_3-Ab, Tz-DBCO (100 eq.), PBS, 4 h at r.t. (ii) [TCO]MSNA (1-8 equiv.), Tz-Ab, PBS, 4 h at r.t.

Reaction mixtures were analysed by SDS-PAGE and native PAGE. As expected, higher equivalents of TCO-MSNA shifted the reaction towards the desired 1:2-Ab-MSNA-ratio specie as seen on both gels (Figure 26). On denaturating conditions the ratio of MSNA-conjugated and unmodified heavy chain shifted towards the conjugated specie when the amount of MSNA was increased. Also on native PAGE the amount of larger molecular weight specie increased proportioned to the amount of MSNA in the reaction mixture. It is notable, that on native PAGE, the molecular mass of the product bands don´t macht the masses indicated by the ladder since the elution of analytes is affected by the shape and charges of the molecules.

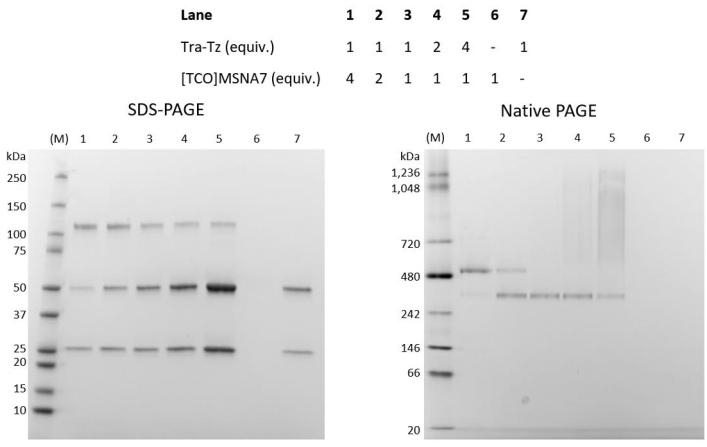

Figure 26. SDS-PAGE analysis of synthesis trials of covalent MSNA-Ab conjugates with mono-TCO MSNA (M): molecular weight ladder.

For larger scale preparation of uniform conjugates, 1:8-Ab:MSNA-ratio was selected for the conjugation reactions. Tetrazine modified **Tz-Tra** or **Tz-IgG** were treated with 8-fold molar excess of **[TCO]MSNA7**, **[TCO]MSNA12** or **[TCO]MSNA13** for 4 h in room temperature after which the reaction mixture was subjected to SEC for purification. The crude product mixture contained also 1:1 ratio conjugate but no unconjugated antibody. Different conjugate species could be separated by SEC. The eluted product fractions overlapped (Figure 27), but the 2:1 ratio MSNA-Ab conjugates could be isolated in relatively high yield (20-26%). In overall, five different Ab-MSNA-conjugates were prepared: **Tra-MSNA7**, **Tra-MSNA12**, **Tra-MSNA13**, **IgG-MSNA7** and **IgG-MSNA13**.

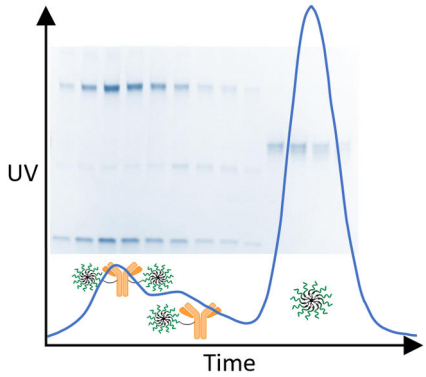

Figure 27. SEC-purification of MSNA-Ab conjugates (**Tra-MSNA7** as an example). SEC chromatogram (blue line) and SDS-PAGE analysis of corresponding SEC fractions overlapped. Adapted from Original Publication **IV**.

3.4.3.6 Characterization of Ab-MSNA conjugates

SDS-PAGE analysis of the purified conjugates showed protein bands at expected molecular weights for unmodified light chain (25 kDa) and MSNA-conjugated heavy chain (120 kDa for non-labelled or 120 kDa for fluorescent labelled conjugates) (Figure 28A). Size-exclusion chromatography equipped with a multiple angle light scattering detector (SEC-MALS) was applied to assess the molecular weight of **Tra-MSNA7**, **Tra-MSNA12** and **IgG-MSNA7**, which were prepared in larger quantity (Figure 28B). Molecular weight estimation with SEC-MALS analysis gave moderate results (Table 4), but in conjunction with SDS-PAGE results the authenticity of the synthesized Ab-MSNA conjugates was confirmed.

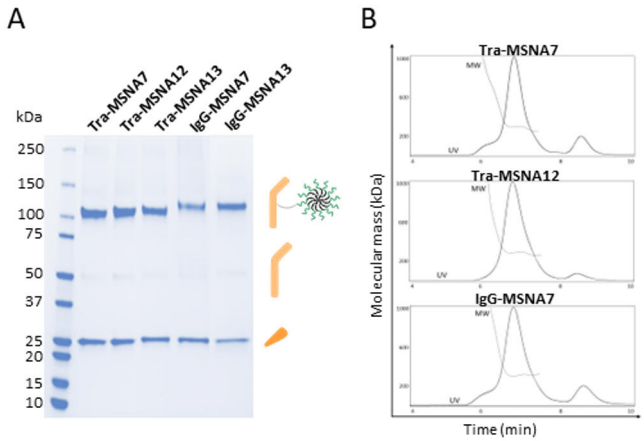

Figure 28. A) SDS-PAGE of **Tra-MSNA7**, **Tra-MSNA12**, **Tra-MSNA13**, **IgG-MSNA7** and **IgG-MSNA13**. **B)** SEC-MALS of **Tra-MSNA7**, **Tra-MSNA12** and **IgG-MSNA7**. Adapted from Original Publication **IV**.

Table 4. Molecular masses of **Tra-MSNA12**, **Tra-MSNA13** and **IgG-MSNA12**

Ab-MSNA conjugate	Calculated molecular mass (kDa)	Observed molecular mass (kDa)
Tra-MSNA7	270.7	289.8±4.1
Tra-MSNA12	270.7	283.3.8±0.6
IgG-MSNA7	268.7	300.7±1.2 kDa

3.4.4 Antigen binding studies with biolayer interferometry

Biolayer interferometry (BLI) was used to study the effect of MSNA conjugation on the Ab´s affinity towards it target protein. Binding experiments with BLI were performed with two assays protocols. For the first experiment (Figure 29A), biotinylated HER2 protein was immobilized to streptavidin sensor. **Tra-MSNA7**, **Tra-MSNA12**, **IgG-MSNA7, [TCO]MSNA7** and **Tra** were used as analytes in 100 nM, 33.3 nM, and 11.1 nM concentrations, and allowed to associate with immobilized HER2 for 300 s followed by 600 s dissociation step. In this experiment, the binding response of **Tra**, **Tra-MSNA7** and **Tra-MSNA12** increased in concentration dependent manner. **IgG-MSNA7** and **[TCO]MSNA7** didn´t bind to sensor which indicates that the binding is due to antibody´s affinity towards the target antigen and not due to the overall structure of the conjugate. For further investigation the assay was reversed, and **Tra**, **Tra-MSNA7** and **Tra-MSNA12** were immobilized to anti-hIgG Fc capture sensors. HER2 protein was used as the analyte in 75 nM, 25 nM, 8.33 nM, 2.78 nM, and 0.93 nM concentrations (Figure 29B). Again 300 s association and 600 s dissociation steps were used. These assays confirmed each

other; trastuzumab and its MSNA conjugates all had affinity towards the HER2-protein and the binding was dependent on concentration. However, the binding of the conjugates is not as high as for the unconjugated antibody which may be caused by the steric and electrostatic interference of the MSNAs to the binding site of the Ab. Overall, these binding experiments demonstrate that affinity towards antigen is retained with high oligonucleotide payload.

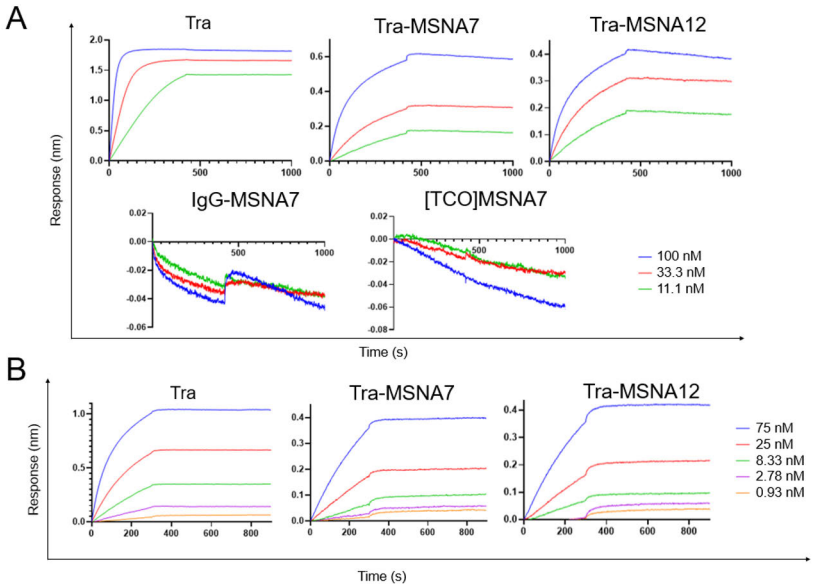

Figure 29. Biolayer interferometry (BLI) experiment to study HER2 binding of the Ab-MSNA conjugates. **A)** biotinylated HER2 immobilized on streptavidin sensor and exposed to **Tra**, **Tra-MSNA7**, **Tra-MSNA12**, **IgG-MSNA7** and **[TCO]MSNA7** as analytes; **B) Tra**, **Tra-MSNA7**, and **Tra-MSNA12** immobilized on anti-hIgG Fc capture sensor and exposed to HER2 as an analyte. Association 300 s and dissociation 600s for both experiments. Adapted from Original Publication **IV**.

3.4.5 Cellular uptake of Ab-MSNA conjugates

3.4.5.1 Fluorescent labelling of trastuzumab

A fluorescently labelled trastuzumab **Tra-Cy5** was synthesized to be used as a reference compound in internalization studies. An activated succinimidyl ester of Cyanine5 was incubated with **Tra** for 4 h at r.t. in 0.1 M sodium borate (pH 8.5). Labelled antibody was purified twice with spin desalting column and recovered in 85% yield based on absorbance at 280 nm. UV-Vis absorbance at 280 and 646 nm was used to determine the degree of labelling (5.8).

3.4.5.2 Cellular uptake of Ab-MSNA conjugates

Antibody mediated cellular uptake (Scheme 8) of the conjugates on BT-474 ductal carcinoma cells was studied with fluorescently labelled conjugates **Tra-MSNA13** and **IgG-MSNA13**. Cyanine5 labelled **[TCO]MSNA13** and **Tra-Cy5** were used as controls. Cells were incubated on ice with 20 nM solutions of **Tra-MSNA13, IgG-MSNA13, [TCO]MSNA13 and Tra-Cy5** for 30 min, after which unbound compounds were washed with ice-cold PBS. Cells were imaged for 16h in two-hour intervals at 37°C 5% CO_2 with a live-cell imaging instrument (Figure 30A-E). Digital phase contrast was used to visualize cells. Fluorescent spots per cell were quantitated with automated software to support the visual observations (Figure 30F). On 0°C only species with affinity towards HER2 on cell surface are bound to cells and when temperature is risen, bound compounds are internalized via receptor mediated endocytosis. At 0-2h, fluorescence signal is seen on the edges of the cells for **Tra-Cy5** and **Tra-MSNA13**. At later time points fluorescence signal spread and moved towards the middle of the cell leading to more countable spots indicating that the compounds are internalized. For **IgG-MSNA13** and **[TCO]MSNA13** no fluorescence signal is observed. In quantitative analysis (Figure 30F), **Tra-MSNA14** seemed to be internalized more rapidly than **Tra-Cy5**, but no real comparison of their internalization kinetics can be made as the compounds are not analogous (labelling site and degree of labelling). These findings suggest that receptor mediated endocytosis works for internalization of high ON load antibody conjugates and supports results of the BLI experiments regarding retained binding affinity.

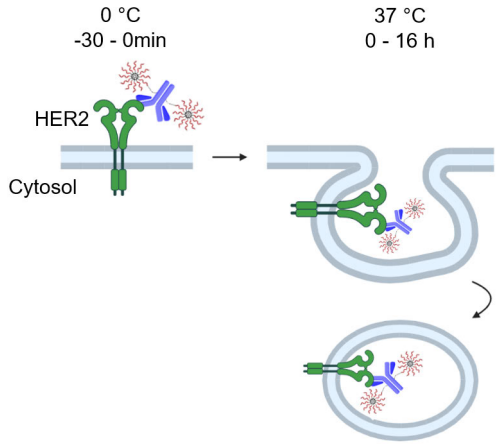

Scheme 8. Schematic overview of reseptor mediated internalization. In 0°C Ab-MSNA is bound to target membrane protein, and when temperature is risen conjugates are internalized.

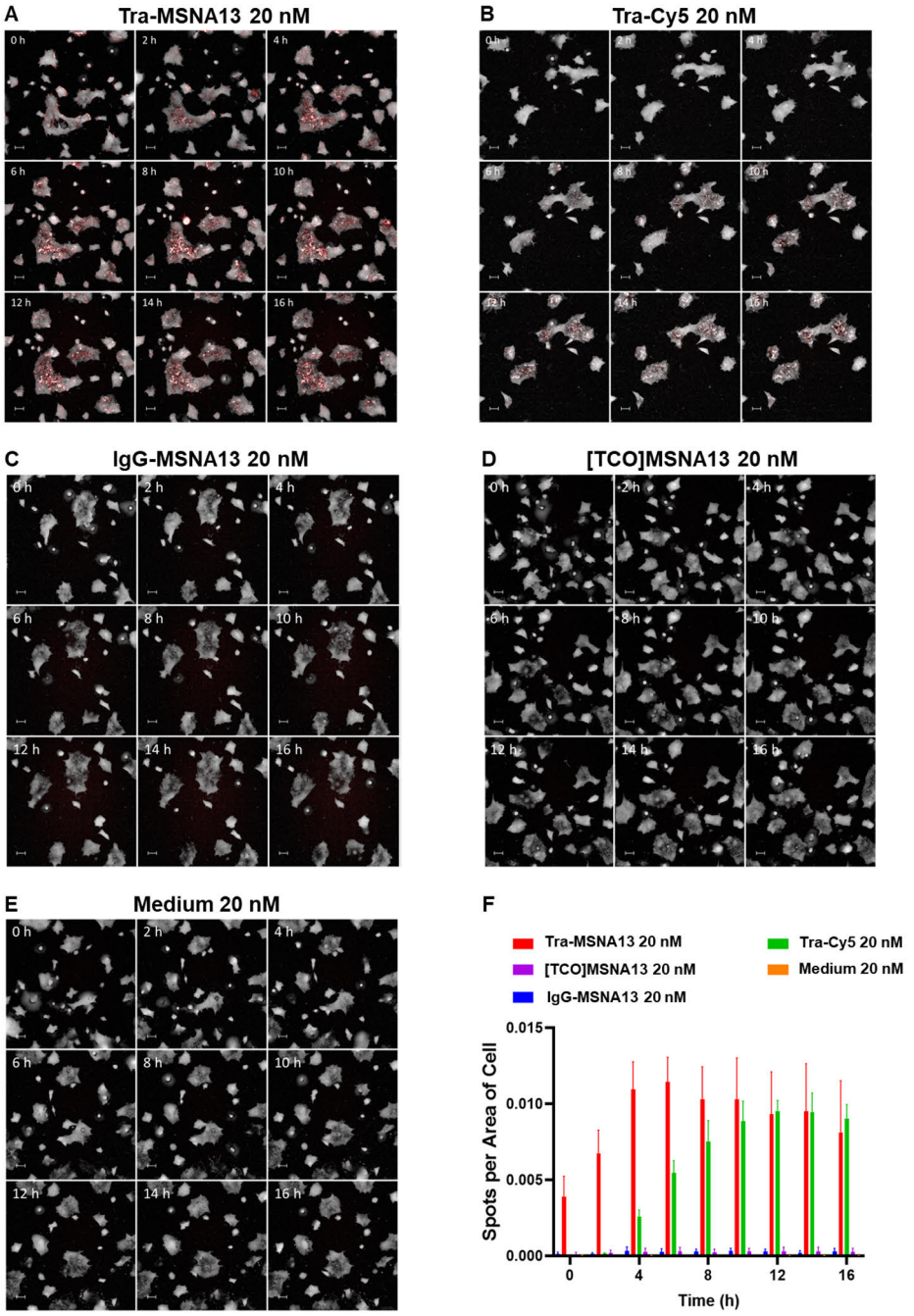

Figure 30. Internalization on BT-474 cells. **A-E)** Channels 647 nm (red) and digital phase contrast combined for representable timeseries images for internalization. **F)** Average number of fluorescent spots (± SD) detected from 647 nm (red) channel per cell detected on phase contrast. Data combined from two replicates. Adapted from Original Publication **IV**.

3.4.6 Effect on the proliferation of breast cancer cells

A label-free live-cell time-lapse imaging was performed to test the effect of the Ab-MSNA conjugates on cancer cell proliferation. BTB-474 cells were seeded in 30% confluency on 96-well plates for 24h prior to experiment. **Tra**, **Tra-MSNA7**, **Tra-MSNA12**, **IgG-MSNA7** and **[TCO]MSNA7** were diluted in culture medium in 0.62-50 concentration, applied on cells and cell proliferation was monitored for 72 h in 37°C 5% CO_2 (Figure 31A). Proliferation of untreated cells was monitored for control. **Tra**, **Tra-MSNA7**, **Tra-MSNA12** inhibited the cell proliferation in similar manner and no anti-proliferative effect was seen with **IgG-MSNA7** and **[TCO]MSNA7**. This indicates that all inhibitory effect is due to interaction of trastuzumab with HER and antiHER2 sequence bearing **MSNA7** doesn´t bring any additional inhibitory properties to the construct. This may be a result of strong anti-proliferative effect of trastuzumab hiding the effects of antiHER2 **MSNA7**, and stable covalent linkage preventing the release of ON payload and preventing it from reaching the target site. Half maximal effective concentrations for **Tra**, **Tra-MSNA7**, **Tra-MSNA12** were 1.28 nM (SEM = 2.13 nM), 1.78 nM (SEM = 0.68 nM), and 2.24 nM (SEM = 0.80 nM), respectively (Figure 31B). These results supported the BLI and fluorescence microscopy results, that MSNA-conjugation doesn´t hamper the antibody´s target recognition properties.

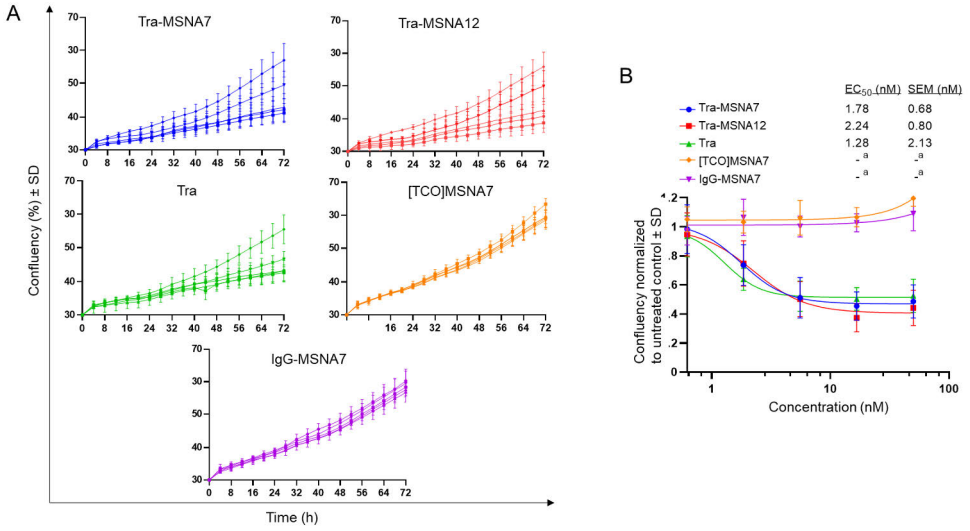

Figure 31. Proliferation of BT-474 cells. **A)** Dose-response curves of **Tra**, **Tra-MSNA7**, **Tra-MSNA12**, **IgG-MSNA7** and **[TCO]MSNA7**. Concentration range 0.62-50 nM. **B)** Dose-response from 72h time point normalized to untreated control (= 1). Half maximal effective inhibitory concentration (EC_{50}) was calculated from the fitted dose-response curves. All measured points are average ± SD of four experiments. [a] EC_{50} value not determinable. Adapted from Original Publication **IV**.

4 Conclusions

An approach for covalent site-specific attachment of a SpyTag002-ON conjugate to various recombinantly produced fusion proteins with Spy/SdyCathcer domain was demonstrated. This developed method is convenient for producing well-defined AOCs in biocompatible conditions. SPAAC-based conjugation and readily accessible azide- and BCN-modified peptide and oligonucleotide intermediates were used to prepare the SpyTag002-ON conjugate in relatively high yield. Antigen recognition properties of the AOCs was demonstrated with TRFIA experiments. The functionality of the AOCs produced by this approach was demonstrated using two immuno-PCR assays for the detection of low-molecular-weight target analytes, MC-LR and E2. Due to the bacterial origin of the SpyCatcher domain, the developed approach is best suited for producing well-defined and stable antibody-oligonucleotide conjugates for *in vitro* assay concepts, although it may also find application in early-stage drug discovery for producing multiple Ab-ON combinations with different binding specificities and/or nucleic acids. In addition to single strand ONs this strategy might be utilized for conjugations of MSNAs and Abs.

A method for the controlled assembly of heterofunctionalized [60]fullerene based molecularly defined MSNAs has been presented. Two consecutive SPAAC-reactions and RP HPLC purifications were applied to obtain MSNAs in relatively high 20-30% yield. The homogeneity and authenticity of the MSNAs were verified by PAGE, MS-ESI spectroscopy, and SEC-MALS. This approach provides a foundation for the addition of labels or organ-specific ligands to MSNAs, as well as their integration with other delivery vehicles.

TCO-modified MSNAs against HER2 mRNA transcripts were synthesized, and specifically ^{18}F-radiolabelld utilizing biocompatible iEDDA reaction. The homogeneity and authenticity of the MSNAs were evaluated using PAGE and SEC-MALS, both before and after radiolabelling. PET/CT was employed to investigate the biodistribution properties of the MSNAs in HER2 expressing HCC1954 tumor-bearing female mice. The effect of PO and PS backbones, different TCO-loadings, and folic acid decoration on biodistribution of MSNAs was evaluated. PS backbone improved stability and increased circulation time. Folate-decoration of PS MSNA

increased tumor accumulation but did not result in an increased tumor/muscle ratio. Higher TCO-content on MSNA increased liver accumulation, which led to reduced distribution to other tissues. These results demonstrate the applicability of MSNAs for site-specific radiolabelling and *in vivo* tracing and serve as a benchmark for i.v.-delivery of DNA-nanomaterials also with integration with tissue-targeting small molecular ligands[151,178,179], aptamers[180,181], and antibodies[182].

Synthesis of molecularly defined Ab-MSNA (1:2) conjugates was described. These conjugates were synthesized in a site-specific manner using biocompatible iEDDA-based conjugation between glycan-engineered antibodies and [60]fullerene-based MSNAs. The resulting conjugates (Ab-ON ratio of 1:24) were isolated in relatively high yield and purity. BLI experiments were used to demonstrate concentration-dependent binding of the conjugates to the target antigen. Fluorescently labelled conjugates were used to show receptor-mediated internalization on BT-474 breast carcinoma cells. Anti-proliferative properties were studied on BT-474 cells using label-free live-cell imaging. In these experiments the conjugates were shown to retain the Ab-mediated target recognition, internalization, and anti-proliferative effects. These promising results suggest further studies with cleavable linker design[183] and/or more active oligonucleotide payloads[184] for a more potent anti-proliferative effect. The synthetic framework could also be utilized for conjugating antibodies to dendritic ONs[130] without the full spherical architecture.

5 Experimental section

5.1 General experimental methods

All reagents and solvents were commercially acquired and used as received. Mass spectra were recorded on a Bruker Daltonics micrOTOF-Q or a Thermo Fisher Scientific hybrid quadrupole Orbitrap mass spectrometer.

5.2 Oligonucleotide synthesis

The oligonucleotides were synthesized on 1-40 μmol scale on an ÄKTA oligopilot plus 10 or Applied Biosystems 3400 automated DNA/RNA synthesizers. Commercially available phosphoramidite building blocks and a conventional phosphoramidite coupling cycle were used for oligonucleotides syntheses. Additional information on the syntheses is given in the results and discussion, as well as in the original publications. Oligonucleotides were purified by RP HPLC, by using a semi-preparative Thermo ODS Hypersil C18 (250 × 10 mm, 5 μm) column, with a gradient elution from 0 to 45% acetonitrile in 50 mmol L^{-1} aqueous triethylammonium acetate over 25 min, flow rate 3.0 mL min^{-1}, UV detection at 260 nm. The product fractions were collected and lyophilized to dryness. The authenticity of the products was verified by MS (ESI-TOF) and isolated yields were determined by UV absorbance at 260 nm.

5.3 Peptide synthesis

The azide modified SpyTag002 peptide was synthesized on a 10 μmol scale on a Rink amide-derived Chem Matrix resin by Applied Biosystems 433A peptide synthesizer. Commercially available amino acid building blocks and a conventional amide coupling cycle were used for the peptide synthesis. The peptide was released from the support using a mixture of anisole and trifluoroacetic acid (TFA), precipitated in cold diethyl ether and purified by RP HPLC, using a semi-preparative Phenomenex Aeris Peptide C18 (250 x 10 mm, 5 μm) column, with a gradient elution from 0 to 100% acetonitrile in 0.1% aqueous TFA over 25 min, flow rate 3.0 mL min^{-1}, UV detection at 280 nm. The product fractions were collected and lyophilized

to dryness. The authenticity of the product was verified by MS (ESI-TOF) and isolated yield was determined by UV absorbance at 280 nm.

5.4 PAGE analysis of MSNAs

A precast 10 x 10 cm Native 6% Tris base, boric acid, EDTA, and acrylamide (TBE) gel (Thermo Fisher Scientific) was fixed into a vertical electrophoresis chamber, and the chamber was filled with running buffer (90 mM Tris, 90 mM borate, and 2 mM EDTA, 8.3 pH). MSNA samples (5 μL of 0.1 μM MSNAs mixed with 5 μL of TBE sample buffer) and a DNA ladder (100, 200···1000 bp) were loaded and electrophoresed at constant 200 V for approximately 30 min. After completion of electrophoresis, gel was removed from the chamber and the MSNA bands were monitored after staining by SYBR™ Gold Nucleic Acid Stain.

5.5 SEC-MALS experiments

SEC-MALS was performed using an Agilent Technologies 1260 Infinity II HPLC system (sampler, pump, and UV–Vis detector) equipped with a Wyatt Technologies miniDAWN light scattering detector and Wyatt Technologies Optilab refractive index detector. An Agilent AdvanceBio SEC 300 Å 2.7 μm 4.6 × 300 mm column and 150 mM sodium phosphate, pH 7.0, as mobile phase eluting at a rate of 0.2 mL min^{-1} and run time of 20 min were used for each experiment. For each run, 10-50 μL of sample with a concentration of 0.1-20 mg mL^{-1} in PBS or Milli-Q water was loaded onto the pre-equilibrated column. An average refractive index increment (dn/dc) of 0.1703 mL g^{-1} was used for the molecular weight calculations.

5.6 SDS-PAGE analysis of Ab-conjugates

Denaturating polyacryl amide gel electrophoresis was used to analyse proteins and antibody conjugates. A precast gel cover (4–15% Mini-PROTEAN® TGX™ Precast Protein, Bio-Rad) was fixed into a vertical electrophoresis chamber, and the running buffer (25 mM Tris, 192 mM glycine, 0.1% SDS, pH 8.3) was filled into the chamber. Samples (mixed with 4x Laemmli Sample buffer, 10% 2-mercaptoethanol) and a protein ladder (Precision Plus Protein Dual Color Standard, Bio-Rad) were loaded and electrophoresed at 200 V for approximately 30 min. After completion of electrophoresis, gel was removed from the chamber and stained with ReadyBlue™ Protein Gel Stain for 2h prior to imaging.

5.7 Native PAGE analysis of Ab-conjugates

Native polyacryl amide gel electrophoresis was used to analyse proteins and antibody conjugates. A precast gel cover (3–12% Bis-Tris, NativePAGE™, Thermo Fisher Scientific) was fixed into a vertical electrophoresis chamber, and the running buffer (NativePAGE™ running buffer, Thermo Fisher Scientific) was filled into the chamber. Samples (mixed with NativePAGE™ sample buffer, Thermo Fisher Scientific) and a protein ladder (NativeMark™, Thermo Fisher Scientific) were loaded and electrophoresed at 200 V for approximately 30 min. After completion of electrophoresis, gel was removed from the chamber and stained with ReadyBlue™ Protein Gel Stain for 2h prior to imaging.

5.8 Cell culture

BT-474 cells were acquired from the American Tissue Culture Collection (ATCC) and cultivated in Gibco DMEM medium with low glucose, GlutaMAX™, and pyruvate (Thermo Fischer Scientific). The medium was supplemented with 10% fetal bovine serum (FBS) and 0.07% insulin. To detach the cells from a T75 flask, 0.25% trypsin was used. The cells were then transferred to new flasks in a 1:3 ratio, and the cell culture was maintained at a temperature of 37°C with a 5% CO2 environment.

5.9 Internalization assay

Cellular experiments were conducted using BT-474 cells. The cells were seeded on a 96-well plate at 30% confluency, 24 hours prior to the experiments. In the internalization assay, fluorescently labelled test items were diluted in Gibco RPMI 1640 (without phenol red) to a concentration of 20 nM. Cells were treated with the prepared solutions and incubated on ice for 30 minutes. Subsequently, the cells were washed twice with ice-cold PBS. Fresh medium was then applied, and the delivery of compounds into the cells was observed for 16 hours at 2-hour intervals using fluorescent microscopy at 649 nm at 37°C 5% CO_2 with live-cell imaging instrument (Operetta, PerkinElmer). Cells were visualized with digital phase contrast.

5.10 Proliferation assay

For the proliferation assay, BT-474 cells were exposed to test items at final concentrations of 0.62, 1.85, 5.56, 16.67, and 50 nM. The cells were monitored for 72 hours at 4-hour intervals using phase contrast microscopy (Incucyte, Sartorius) at temperature of 37°C and 5% CO2. Confluency values were calculated from the obtained images using software provided with the instrument.

5.11 Biolayer interferometry experiments

The experiments were performed using FortéBio's Octet RED96e biolayer interferometry (BLI) biosensor instrument. Two assay methods were employed. In assay method one, the streptavidin (SA) sensors from Sartorius were loaded with biotinylated-HER2 for a duration of 300 seconds. Following this, the HER2-loaded SA sensors were immersed in 1× Octet kinetics buffer from Sartorius for 60 seconds to establish a baseline. Subsequently, the sensors were exposed to each analyte solution (ranging from 11.1 to 100 nM in Octet kinetics buffer) for 300 seconds to facilitate association. The dissociation phase was then carried out in kinetics buffer for 600 seconds. In assay method two, the anti-humanIgG FC capture (AHC) sensors from Sartorius were loaded with test items for 300 seconds. After loading, the AHC sensors were immersed in 1× Octet kinetics buffer for 60 seconds to establish a baseline. The sensors were then exposed to HER2 solution (ranging from 0.93 to 75 nM in kinetics buffer) for 300 seconds to facilitate association. The dissociation phase was carried out in kinetics buffer for 600 seconds.

Acknowledgemets

This thesis is based on experimental work conducted in the Laboratory of Organic Chemistry and Chemical Biology at the Department of Chemistry, University of Turku and at the R&D of Orion Pharma, Turku. Financial support from Business Finland and Orion Pharma are gratefully acknowledged. My doctoral training was done in the industrial PhD (iPhD) track of Drug Research Doctoral Program (DRDP), and I want to thank DRDP and Orion Pharma for initiating this wonderful opportunity for young researchers to gain industry experience.

I express my deepest gratitude to professor Pasi Virta for being my research director. Pasi is a professor who does not run out of ideas and research questions. Luckily, we found enough answers to put this thesis in covers. Thank you also Dr. Harri Salo and Dr. Olli Törmäkangas for being my thesis supervisors at Orion. You three gave me enough freedom to learn by doing and did not micro-manage which I find a very deep indication of trust.

I wish to acknowledge professor Jørgen Kjems and professor Poul Nielsen who reviewed this thesis. I also thank professor Mauri Kostiainen for accepting the role of my opponent in the dissertation defence. Thank you professor Urpo Lamminmäki for giving expert advice as a member of my follow-up comittee. Thank you Dr. Tuomas Huovinen for your comments on the thesis. Thank you Jyrki Lehtimäki for looking after me at Orion.

Publications included in this thesis are supported and co-authored by many other investigators who I would like to aknowledge: Tatsiana Auchynnikava, Dr. Olli Moisio, Heidi Liljenbäck, Andriana Putri, Imran Iqbal, professor Anne Roivainen and professor Anu Airaksinen from Turku PET Centre; Dr. Vijay Gulumkar and Anastasiia Kushnarova-Vakal from University of Turku; Dr. Johan Rajander and Dr. Jani Rahkila from Åbo Akademi; Dr. Elina Vuorimaa-Laukkanen from Tampere University; professor Tapani Viitala and professor Marjo Yliperttula from University of Helsinki.

I wish to thank all the members of the Bioorganic Group with whom I have worked during my doctoral studies: Aapo Aho, Dr. Asmo Aro-Heinilä, Dr. Dattatraya Ukale, Dr. Tharun Kotammagari, Dr. Vijay Gulumkar, Dr. Ville Tähtinen, Dr. Heidi Korhonen, Lange Saleh, Dr. Madhuri Hande, Mark Afari, Dr.

Mikko Ora, Dr. Päivi Poijärvi-Virta, Dr. Satu Mikkola, associate professor Tuomas Lönnberg, Dr. Petja Rosenqvist, Petteri Lepistö, Dr. Sajal Maity, Tommi Österlund and Toni Laine. Special thanks to Aapo, Asmo, Ville and Petja who I consider my good friends and who has shared many therapeutic laughters with me, mostly in situations where there was no reason. Special-special thanks to Aapo for many shared giggles and countles memes on the whiteboard in our shared office at Arcanum. Thanks to Dr. Tuomas Karskela and Dr. Alex Dickens for their support with instruments. Thank you Kirsi Laaksonen, Tiina Buss, Kari Loikas and Mauri Nauma for your help with laboratory equipment, IT systems and chemicals.

During my time at Orion I got to meet research professionals who helped and taught me a lot. Thank you especially Laura Leimu, Satu Kaskinoro, Anja Vilkman, Dr. Victor Nesati, Dr. Kati Räsänen, Patrik Holm and Camilla Ahlqvist for all your help and valuable lessons on new laboratory techniques. Thank you Olli Huhtinen, Dr. Antti Kulmala, Dr. Markus Nurmi and Emilia Kettunen, who might have not been that involved in the research I did, but with whom I have shared many joyful moments at work and on free time. Additionally, I want to aknowledge everyone working in Turla who has shared the ups and downs of research and life with me.

I want to also thank all my fellow students of the DRDP for extra-currilucar activities at the DRDP annual meetings, christmas parties and other night outs. Especially Anna, Emmi and Olli, thanks for the red wine.

Thank you Juuso, Milla, Sini and Sampo for your friendship and many shared memories. I wish to thank my friends since chilhood, Taneli, Juho-Arttu, Ville and Joonas for all the memories and in the recent years the annual autumn get-aways in the bushes. Thank you also Valtteri for your longlasting friendship.

Thank you mom and dad for helping me during my educational path. Thanks to my sister Eeva for engouragement and showing the example of going to university. Thank you family Haravuori for all the support and warm memories.

This list of aknowledgements is far from complete. If you are reading this and feel that you have supported me, please have my sincerest gratitude. I am happy that everyday I am surrounded by people who are willing to lend their expertise, listen and offer kind and engouraging words. We are nothing without others.

I am forever grateful for the support of my darling wife Eveliina, to whom I have trusted when I have had doubts and who has rejoiced with me whenever there was a reason. Every morning, I'm filled with warm joy to wake up next to you.

Turku, September 2023

Antti Äärelä

List of References

(1) Hammond, S. M., Aartsma-Rus, A., Alves, S., Borgos, S. E., Buijsen, R. A. M., Collin, R. W. J., Covello, G., Denti, A. M., Lourdes, R. D., Echevarria, L., Foged, C., Gaina, G., Garanto, A., Goyenvalle, A. T., Guzowska, M., Holodnuka, I., Jones, D. R., Krause, S., Lehto, T., Montolio, M., Roon-Mom, W. Van, Arechavala-Gomeza, V. *EMBO Mol. Med.* **2021**, *13*, e13243.

(2) Roberts, T. C., Langer, R., Wood, M. J. A. *Nat. Rev. Drug Discov.* **2020**, *19* (10), 673–694.

(3) Reese, C. B. *Org. Biomol. Chem.* **2005**, *3* (21), 3851–3868.

(4) Palluk, S., Arlow, D. H., De Rond, T., Barthel, S., Kang, J. S., Bector, R., Baghdassarian, H. M., Truong, A. N., Kim, P. W., Singh, A. K., Hillson, N. J., Keasling, J. D. *Nat. Biotechnol.* **2018**, *36* (7), 645–650.

(5) Roberts, T. C., Langer, R., Wood, M. J. A. *Nat. Rev. Drug Discov.* **2020**, *19* (10), 673–694.

(6) Kim, J., Hu, C., Moufawad El Achkar, C., Black, L. E., Douville, J., Larson, A., Pendergast, M. K., Goldkind, S. F., Lee, E. A., Kuniholm, A., Soucy, A., Vaze, J., Belur, N. R., Fredriksen, K., Stojkovska, I., Tsytsykova, A., Armant, M., DiDonato, R. L., Choi, J., Cornelissen, L., Pereira, L. M., Augustine, E. F., Genetti, C. A., Dies, K., Barton, B., Williams, L., Goodlett, B. D., Riley, B. L., Pasternak, A., Berry, E. R., Pflock, K. A., Chu, S., Reed, C., Tyndall, K., Agrawal, P. B., Beggs, A. H., Grant, P. E., Urion, D. K., Snyder, R. O., Waisbren, S. E., Poduri, A., Park, P. J., Patterson, A., Biffi, A., Mazzulli, J. R., Bodamer, O., Berde, C. B., Yu, T. W. *N. Engl. J. Med.* **2019**, *381* (17), 1644–1652.

(7) Brad Wan, W., Seth, P. P. *J. Med. Chem.* **2016**, *59* (21), 9645–9667.

(8) Hong, S., Sun, N., Liu, M., Wang, J., Pei, R. *RSC Adv.* **2016**, *6* (113), 112445–112450.

(9) White, R. R., Sullenger, B. A., Rusconi, C. P. *J. Clin. Invest.* **2000**, *106* (8), 929–934.

(10) Grillone, L. R., Lanz, R. *Drugs of Today* **2001**, *37* (4), 245–255.

(11) Geary, R. S., Henry, S. P., Grillone, L. R. *Clin. Pharmacokinet.* **2002**, *41* (4), 255–260.

(12) Rubinsztein, D. C., Codogno, P., Levine, B. *Nat. Rev. Drug Discov.* **2012**, *11* (9), 709–730.

(13) Igarashi, J., Niwa, Y., Sugiyama, D. *Futur. Rare Dis.* **2022**, *2* (1).

(14) Crooke, S. T. *Nucleic Acid Ther.* **2017**, *27* (2), 70–77.

(15) Wu, H., Lima, W. F., Zhang, H., Fan, A., Sun, H., Crooke, S. T. *J. Biol. Chem.* **2004**, *279* (17), 17181–17189.

(16) Lebedeva, I., Stein, C. A. *Annu. Rev. Pharmacol. Toxicol.* **2001**, *41*, 403–419.

(17) Yoshida, T., Naito, Y., Yasuhara, H., Sasaki, K., Kawaji, H., Kawai, J., Naito, M., Okuda, H., Obika, S., Inoue, T. *Genes to Cells* **2019**, *24* (12), 827–835.

(18) Liang, X. H., Sun, H., Nichols, J. G., Crooke, S. T. *Mol. Ther.* **2017**, *25* (9), 2075–2092.

(19) Lennox, K. A., Behlke, M. A. *Nucleic Acids Res.* **2016**, *44* (2), 863–877.

(20) Ravindra N. Singh, Singh and Natalia N. *Adv. Neurobiol.* **2018**, *20*, 31–61.

(21) Dominski, Z., Kole, R. *Proc. Natl. Acad. Sci. U. S. A.* **1993**, *90* (18), 8673–8677.

(22) Aartsma-Rus, A., Straub, V., Hemmings, R., Haas, M., Schlosser-Weber, G., Stoyanova-Beninska, V., Mercuri, E., Muntoni, F., Sepodes, B., Vroom, E., Balabanov, P. *Nucleic Acid Ther.* **2017**, *27* (5), 251–259.

(23) Wan, L., Dreyfuss, G. *Cell* **2017**, *170* (1), 5.

(24) Ward, A. J., Norrbom, M., Chun, S., Bennett, C. F., Rigo, F. *Nucleic Acids Res.* **2014**, *42* (9), 5871–5879.
(25) Tuschl, T., Elbashir, S. M., Harborth, J., Lendeckel, W., Yalcin, A., Weber, K. *Nature* **2001**, *411*, 494–498.
(26) Kim, D. H., Behlke, M. A., Rose, S. D., Chang, M. S., Choi, S., Rossi, J. J. *Nat. Biotechnol.* **2005**, *23* (2), 222–226.
(27) Schürmann, N., Trabuco, L. G., Bender, C., Russell, R. B., Grimm, D. *Nat. Struct. Mol. Biol.* **2013**, *20* (7), 818–826.
(28) Roberts, T. C. In *Advances in Experimental Medicine and Biology*, 2015, Vol. 887, pp 15–30.
(29) Beccaria et al., Bracaglia. *Physiol. Behav.* **2017**, *176* (5), 139–148.
(30) Okada, N., Lin, C. P., Ribeiro, M. C., Biton, A., Lai, G., He, X., Bu, P., Vogel, H., Jablons, D. M., Keller, A. C., Erby Wilkinson, J., He, B., Speed, T. P., He, L. *Genes Dev.* **2014**, *28* (5), 438–450.
(31) Bueno, M. J., Malumbres, M. *Biochim. Biophys. Acta* **2011**, *1812* (5), 592–601.
(32) Shimakami, T., Yamane, D., Jangra, R. K., Kempf, B. J., Spaniel, C., Barton, D. J., Lemon, S. M. *PNAS* **2012**, *109* (3), 941–946.
(33) Balasubramaniam, M., Pandhare, J., Dash, C. *Viruses* **2018**, *10* (3), 1–35.
(34) Xu, S. J., Hu, H. T., Li, H. L., Chang, S. *Cells* **2019**, *8*, 1140.
(35) Wendt, A., Esguerra, J. L., Eliasson, L. *Curr. Opin. Pharmacol.* **2018**, *43*, 46–52.
(36) Vienberg, S., Geiger, J., Madsen, S., Dalgaard, L. T. *Acta Physiol.* **2017**, *219* (2), 346–361.
(37) Chen, J. F., Tao, Y., Li, J., Deng, Z., Yan, Z., Xiao, X., Wang, D. Z. *J. Cell Biol.* **2010**, *190* (5), 867–879.
(38) van Rooij, E., Liu, N., Olson, E. N. *Trends Genet.* **2008**, *24* (4), 159–166.
(39) Cacchiarelli, D., Martone, J., Girardi, E., Cesana, M., Incitti, T., Morlando, M., Nicoletti, C., Santini, T., Sthandier, O., Barberi, L., Auricchio, A., Musar, A., Bozzoni, I. *Cell Metab.* **2010**, *12* (4), 341–351.
(40) Roberts, T. C., Blomberg, K. E. M., McClorey, G., Andaloussi, S. El, Godfrey, C., Betts, C., Coursindel, T., Gait, M. J., Smith, C. E., Wood, M. J. *Mol. Ther. - Nucleic Acids* **2012**, *1* (8), e39.
(41) Krützfeldt, J., Rajewsky, N., Braich, R., Rajeev, K. G., Tuschl, T., Manoharan, M., Stoffel, M. *Nature* **2005**, *438* (7068), 685–689.
(42) Lindow, M., Kauppinen, S. *J. Cell Biol.* **2012**, *199* (3), 407–412.
(43) Choi, W. Y., Giraldez, A. J., Schier, A. F. *Science (80-.).* **2007**, *318* (5848), 271–274.
(44) Wang, Z. In *Methods in Molecular Biology*, 2011, Vol. 676, pp 43–49.
(45) Tuerk, C., Gold, L. *Science (80-.).* **1990**, *249* (4968), 505–510.
(46) Ellington, A. D., Szostak, J. W. *Nature* **1990**, *346* (6287), 818–822.
(47) Santner, T., Rieder, U., Kreutz, C., Micura, R. *J. Am. Chem. Soc.* **2012**, *134* (29), 11928–11931.
(48) Hu, J., Wang, T., Kim, J., Shannon, C., Easley, C. J. *J. Am. Chem. Soc.* **2012**, *134* (16), 7066–7072.
(49) Davies, D. R., Gelinas, A. D., Zhang, C., Rohloff, J. C., Carter, J. D., O'Connell, D., Waugh, S. M., Wolk, S. K., Mayfield, W. S., Burgin, A. B., Edwards, T. E., Stewart, L. J., Gold, L., Janjic, N., Jarvis, T. C. *PNAS* **2012**, *109* (49), 19971–19976.
(50) Kreutz, C., Kählig, H., Konrat, R., Micura, R. *Angew. Chemie - Int. Ed.* **2006**, *45* (21), 3450–3453.
(51) Liu, M., Yang, T., Chen, Z., Wang, Z., He, N. *Biomater. Sci.* **2018**, *6* (12), 3152–3159.
(52) Zhang, K., Sefah, K., Tang, L., Zhao, Z., Zhu, G., Ye, M., Sun, W., Goodison, S., Tan, W. *ChemMedChem* **2012**, *7* (1), 79–84.
(53) Pfeiffer, F., Mayer, G. *Front. Chem.* **2016**, *4*, 1–21.
(54) Röthlisberger, P., Gasse, C., Hollenstein, M. *Int. J. Mol. Sci.* **2017**, *18* (11).
(55) Hua, X., Zhou, Z., Yuan, L., Liu, S. *Anal. Chim. Acta* **2013**, *788*, 135–140.

(56) Liu, Z., Duan, J. H., Song, Y. M., Ma, J., Wang, F. D., Lu, X., Yang, X. Da. *J. Transl. Med.* **2012**, *10* (1), 1.
(57) Cummins, L. L., Owens, S. R., Risen, L. M., Lesnik, E. A., Freier, S. M., Mc Gee, D., Cook, C. J., Cook, P. D. *Nucleic Acids Res.* **1995**, *23* (11), 2019–2024.
(58) Monia, B. P., Johnston, J. F., Sasmor, H., Cummins, L. L. *J. Biol. Chem.* **1996**, *271* (24), 14533–14540.
(59) Martin, P. *ChemInform* **2010**, *26* (31).
(60) Khvorova, A., Watts, J. K. *Nat. Biotechnol.* **2017**, *35* (3), 238–248.
(61) Singh, S. K., Nielsen, P., Koshkin, A. a., Wengel, J. *Chem. Commun.* **1998**, 455–456.
(62) Karima, R., Aurelie, G. In *Exon Skipping and Inclusion Therapies*, 2018, pp 381–394.
(63) Watts, J. K. *Chem. Commun.* **2013**, *49* (50), 5618–5620.
(64) Eckstein, F. *Nucleic Acid Ther.* **2014**, *24* (6), 374–387.
(65) Nielsen, P. E., Egholm, M., Berg, R. H., Buchardt O. *Science.* 1991, p 1497.
(66) Summerton, J., Weller, D. *Antisense Nucleic Acid Drug Dev.* **1997**, *7* (3), 187–195.
(67) Lundin, K. E., Gissberg, O., Smith, C. I. E. *Hum. Gene Ther.* **2015**, *26* (8), 475–485.
(68) Geary, R. S. *Expert Opin. Drug Metab. Toxicol.* **2009**, *5* (4), 381–391.
(69) Juliano, R., Bauman, J., Kang, H., Ming, X. *Mol. Pharm.* **2009**, *6* (3), 686–695.
(70) Levin, A. A., Yu, R. Z., Geary, R. S. In *Antisense Drug Technology: Principles, Strategies, and Applications, Second Edition*, CRC Press, 2007, pp 183–215.
(71) Andersson, P. In *Methods in Molecular Biology*, 2022, Vol. 2434, pp 355–370.
(72) Stebbins, C. C., Petrillo, M., Stevenson, L. F. *Bioanalysis* **2019**, *11* (21), 1913–1916.
(73) Karikó, K., Muramatsu, H., Welsh, F. A., Ludwig, J., Kato, H., Akira, S., Weissman, D. *Mol. Ther.* **2008**, *16* (11), 1833–1840.
(74) Karikó, K., Buckstein, M., Ni, H., Weissman, D. *Immunity* **2005**, *23* (2), 165–175.
(75) Morais, P., Adachi, H., Yu, Y. T. *Front. Cell Dev. Biol.* **2021**, *9*, 1–9.
(76) Mirkin, C. A., Letsinger, R. L., Mucic, R. C., Storhoff, J. J. *Nature* **1996**, *382* (6592), 607–609.
(77) Li, Z., Jin, R., Mirkin, C. A., Letsinger, R. L. *Nucleic Acids Res.* **2002**, *30* (7), 1558–1562.
(78) Letsinger RL, Mirkin CA, Elghanian R, Mucic RC, S. J. *Sulfur Silicon Relat Elem.* **1999**, *144* (1), 359–362.
(79) Zhang, C., MacFarlane, R. J., Young, K. L., Choi, C. H. J., Hao, L., Auyeung, E., Liu, G., Zhou, X., Mirkin, C. A. *Nat. Mater.* **2013**, *12* (8), 741–746.
(80) Cutler, J. I., Zheng, D., Xu, X., Giljohann, D. A., Mirkin, C. A. *Nano Lett.* **2010**, *10* (4), 1477–1480.
(81) Lee, J. S., Lytton-Jean, A. K. R., Hurst, S. J., Mirkin, C. A. *Nano Lett.* **2007**, *7* (7), 2112–2115.
(82) Li, H., Zhang, B., Lu, X., Tan, X., Jia, F., Xiao, Y., Cheng, Z., Li, Y., Silva, D. O., Schrekker, H. S., Zhang, K., Mirkin, C. A. *PNAS* **2018**, *115* (17), 4340–4344.
(83) Zhang, C., Hao, L., Calabrese, C. M., Zhou, Y., Choi, C. H. J., Xing, H., Mirkin, C. A. *Small* **2015**, *11* (40), 5360–5368.
(84) Alemdaroglu, F. E., Alemdaroglu, N. C., Langguth, P., Herrmann, A. *Adv. Mater.* **2008**, *20* (5), 899–902.
(85) Bousmail, D., Amrein, L., Fakhoury, J. J., Fakih, H. H., Hsu, J. C. C., Panasci, L., Sleiman, H. F. *Chem. Sci.* **2017**, *8* (9), 6218–6229.
(86) Rush, A. M., Nelles, D. A., Blum, A. P., Barnhill, S. A., Tatro, E. T., Yeo, G. W., Gianneschi, N. C. *J. Am. Chem. Soc.* **2014**, *136* (21), 7615–7618.
(87) Tan, X., Lu, X., Jia, F., Liu, X., Sun, Y., Logan, J. K., Zhang, K. *J. Am. Chem. Soc.* **2016**, *138* (34), 10834–10837.
(88) Barnaby, S. N., Sita, T. L., Petrosko, S. H., Stegh, A. H., Mirkin, C. A. In *Cancer Treatment and Research*, 2015, Vol. 166, pp 23–50.
(89) Massich, M. D., Giljohann, D. A., Seferos, D. S., Ludlow, L. E., Horvath, C. M., Mirkin, C. A. *Mol. Pharm.* **2009**, *6* (6), 1934–1940.

(90) Kyriazi, M. E., El-Sagheer, A. H., Medintz, I. L., Brown, T., Kanaras, A. G. *Bioconjug. Chem.* **2022**, *33* (1), 219–225.
(91) Song, Y., Song, W., Lan, X., Cai, W., Jiang, D. *Aggregate* **2022**, *3* (1).
(92) Kapadia, C. H., Melamed, J. R., Day, E. S. *BioDrugs* **2018**, *32* (4), 297–309.
(93) Mahajan, A. S., Stegh, A. H. *Cancers (Basel).* **2022**, *14* (7), 1615.
(94) Bousmail, D., Amrein, L., Fakhoury, J. J., Fakih, H. H., Hsu, J. C. C., Panasci, L., Sleiman, H. F. *Chem. Sci.* **2017**, *8* (9), 6218–6229.
(95) Zhang, X. Q., Xu, X., Lam, R., Giljohann, D., Ho, D., Mirkin, C. A. *ACS Nano* **2011**, *5* (9), 6962–6970.
(96) Kusmierz, C. D., Bujold, K. E., Callmann, C. E., Mirkin, C. A. *ACS Cent. Sci.* **2020**, *6* (5), 815–822.
(97) Brodin, J. D., Sprangers, A. J., McMillan, J. R., Mirkin, C. A. *J. Am. Chem. Soc.* **2015**, *137* (47), 14838–14841.
(98) Giljohann, D. A., Seferos, D. S., Patel, P. C., Millstone, J. E., Rosi, N. L., Mirkin, C. A. *Nano Lett.* **2007**, *7* (12), 3818–3821.
(99) Ferrer, J. R., Sinegra, A. J., Ivancic, D., Yeap, X. Y., Qiu, L., Wang, J. J., Zhang, Z. J., Wertheim, J. A., Mirkin, C. A. *ACS Nano* **2020**, *14* (2), 1682–1693.
(100) Rosi, N. L., Giljohann, D. A., Thaxton, C. S., Lytton-Jean, A. K. R., Han, M. S., Mirkin, C. A. *Science (80-.).* **2006**, *312* (5776), 1027–1030.
(101) Patel, P. C., Giljohann, D. A., Daniel, W. L., Zheng, D., Prigodich, A. E., Mirkin, C. A. *Bioconjug. Chem.* **2010**, *21* (12), 2250–2256.
(102) Choi, C. H. J., Hao, L., Narayan, S. P., Auyeung, E., Mirkin, C. A. *PNAS* **2013**, *110* (19), 7625–7630.
(103) Pearson, A. M., Rich, A., Krieger, M. *J. Biol. Chem.* **1993**, *268* (5), 3546–3554.
(104) Arnott, S., Chandrasekaran, K., Marttila, C. M. *Biochem. J.* **1974**, *141* (2), 537–543.
(105) Blanco, E., Shen, H., Ferrari, M. *Nat. Biotechnol.* **2015**, *33* (9), 941–951.
(106) Tavares, A. J., Poon, W., Zhang, Y. N., Dai, Q., Besla, R., Ding, D., Ouyang, B., Li, A., Chen, J., Zheng, G., Robbins, C., Chan, W. C. W., Murphy, C. J. *PNAS* **2017**, *114* (51), E10871–E10880.
(107) Tsoi, K. M., Macparland, S. A., Ma, X. Z., Spetzler, V. N., Echeverri, J., Ouyang, B., Fadel, S. M., Sykes, E. A., Goldaracena, N., Kaths, J. M., Conneely, J. B., Alman, B. A., Selzner, M., Ostrowski, M. A., Adeyi, O. A., Zilman, A., McGilvray, I. D., Chan, W. C. W. *Nat. Mater.* **2016**, *15* (11), 1212–1221.
(108) Tan, J., Shah, S., Thomas, A., Ou-Yang, H. D., Liu, Y. *Microfluid. Nanofluidics* **2013**, *14* (1–2), 77–87.
(109) Decuzzi, P., Lee, S., Bhushan, B., Ferrari, M. *Ann. Biomed. Eng.* **2005**, *33* (2), 179–190.
(110) Shah, S., Liu, Y., Hu, W., Gao, J. *J. Nanosci. Nanotechnol.* **2011**, *11* (2), 919–928.
(111) Matsumura, Y., Maeda, H. *Cancer Res.* **1986**, *46* (8), 6387–6392.
(112) Heldin, C., Rubin, K., Pietras, K., Östman, A. **2004**, *4*, 806–813.
(113) Chauhan, V. P., Stylianopoulos, T., Martin, J. D., PopoviÄ, Z., Chen, O., Kamoun, W. S., Bawendi, M. G., Fukumura, D., Jain, R. K. *Nat. Nanotechnol.* **2012**, *7* (6), 383–388.
(114) Monsky, W. L., Fukumura, D., Gohongi, T., Ancukiewcz, M., Weich, H. A., Torchilin, V. P., Yuan, F., Jain, R. K. *Cancer Res.* **1999**, *59* (16), 4129–4135.
(115) Jain, R. K., Stylianopoulos, T. *Nat. Rev. Clin. Oncol.* **2010**, *7* (11), 653–664.
(116) Gratton, S. E. A., Ropp, P. A., Pohlhaus, P. D., Luft, J. C., Madden, V. J., Napier, M. E., DeSimone, J. M. *PNAS* **2008**, *105* (33), 11613–11618.
(117) Serda, R. E., Gu, J., Bhavane, R. C., Liu, X. W., Chiappini, C., Decuzzi, P., Ferrari, M. *Biomaterials* **2009**, *30* (13), 2440–2448.
(118) Lee, Y., Fukushima, S., Bae, Y., Hiki, S., Ishii, T., Kataoka, K. *J. Am. Chem. Soc.* **2007**, *129* (17), 5362–5363.
(119) Chinen, A. B., Guan, C. M., Ko, C. H., Mirkin, C. A. *Small* **2017**, *13* (16), 1603847.

(120) Jensen, S. A., Day, E. S., Ko, C. H., Hurley, L. A., Luciano, J. P., Kouri, F. M., Merkel, T. J., Luthi, A. C., Patel, P. C., Cutler, J. I., Daniel, W. L., Scott, A. W., Rotz, M. W., Meade, T. J., Giljohann, D. A., Mirkin, C. A., Stegh, A. H. *Sci. Transl. Med.* **2013**, *5* (209), 209ra152.
(121) Xiao, F., Lin, L., Chao, Z., Shao, C., Chen, Z., Wei, Z., Lu, J., Huang, Y., Li, L., Liu, Q., Liang, Y., Tian, L. *Angew. Chemie - Int. Ed.* **2020**, *59* (24), 9702–9710.
(122) Sita, T. L., Kouri, F. M., Hurley, L. A., Merkel, T. J., Chalastanis, A., May, J. L., Ghelfi, S. T., Cole, L. E., Cayton, T. C., Barnaby, S. N., Sprangers, A. J., Savalia, N., James, C. D., Lee, A., Mirkin, C. A., Stegh, A. H. *PNAS* **2017**, *114* (16), 4129–4134.
(123) Kumthekar, P., Ko, C. H., Paunesku, T., Dixit, K., Sonabend, A. M., Bloch, O., Tate, M., Schwartz, M., Zuckerman, L., Lezon, R., Lukas, R. V., Jovanovic, B., McCortney, K., Colman, H., Chen, S., Lai, B., Antipova, O., Deng, J., Li, L., Tommasini-Ghelfi, S., Hurley, L. A., Unruh, D., Sharma, N. V., Kandpal, M., Kouri, F. M., Davuluri, R. V., Brat, D. J., Muzzio, M., Glass, M., Vijayakumar, V., Heidel, J., Giles, F. J., Adams, A. K., James, C. D., Woloschak, G. E., Horbinski, C., Stegh, A. H. *Sci. Transl. Med.* **2021**, *13* (584), 3945.
(124) Huynh, E., Zheng, G. *Nanomedicine* **2015**, *10* (13), 1993–1995.
(125) Hansen, A. E., Petersen, A. L., Henriksen, J. R., Boerresen, B., Rasmussen, P., Elema, D. R., Rosenschöld, P. M. A., Kristensen, A. T., Kjær, A., Andresen, T. L. *ACS Nano* **2015**, *9* (7), 6985–6995.
(126) Yougen, L. I., Tseng, Y. D., Kwon, S. Y., D'Espaux, L., Bunch, J. S., McEuen, P. L., Luo, D. *Nat. Mater.* **2004**, *3* (1), 38–42.
(127) Qu, Y., Yang, J., Zhan, P., Liu, S., Zhang, K., Jiang, Q., Li, C., Ding, B. *ACS Appl. Mater. Interfaces* **2017**, *9* (24), 20324–20329.
(128) Caruthers, M. H. *J. Biol. Chem.* **2013**, *288* (2), 1420–1427.
(129) Shchepinov, M. S., Udalova, I. A., Bridgman, A. J., Southern, E. M. *Nucleic Acids Res.* **1997**, *25* (22), 4447–4454.
(130) Distler, M. E., Teplensky, M. H., Bujold, K. E., Kusmierz, C. D., Evangelopoulos, M., Mirkin, C. A. *J. Am. Chem. Soc.* **2021**, *143* (34), 13513–13518.
(131) Tewabe, A., Abate, A., Tamrie, M., Seyfu, A., Siraj, E. A. *J. Multidiscip. Healthc.* **2021**, *14*, 1711–1724.
(132) Mullard, A. *Nat. Rev. Drug Discov.* **2022**, *21* (1), 6–8.
(133) Dovgan, I., Koniev, O., Kolodych, S., Wagner, A. *Bioconjug. Chem.* **2019**, *30* (10), 2483–2501.
(134) Song, E., Zhu, P., Lee, S. K., Chowdhury, D., Kussman, S., Dykxhoorn, D. M., Feng, Y., Palliser, D., Weiner, D. B., Shankar, P., Marasco, W. A., Lieberman, J. *Nat. Biotechnol.* **2005**, *23* (6), 709–717.
(135) Serrano Cardona, L., Muñoz Mata, E. *Early Hum. Dev.* **2013**, *83* (1), 1–11.
(136) Li, G., Moellering, R. E. *ChemBioChem* **2019**, *20* (12), 1599–1605.
(137) Hsu, N. S., Lee, C. C., Kuo, W. C., Chang, Y. W., Lo, S. Y., Wang, A. H. J. *Bioconjug. Chem.* **2020**, *31* (7), 1804–1811.
(138) Dugal-Tessier, J., Thirumalairajan, S., Jain, N. *J. Clin. Med.* **2021**, *10* (4), 1–17.
(139) Zhang, K., Hao, L., Hurst, S. J., Mirkin, C. A. *J. Am. Chem. Soc.* **2012**, *134* (40), 16488–16491.
(140) Viney, N. J., van Capelleveen, J. C., Geary, R. S., Xia, S., Tami, J. A., Yu, R. Z., Marcovina, S. M., Hughes, S. G., Graham, M. J., Crooke, R. M., Crooke, S. T., Witztum, J. L., Stroes, E. S., Tsimikas, S. *Lancet* **2016**, *388* (10057), 2239–2253.
(141) Zimmermann, T. S., Karsten, V., Chan, A., Chiesa, J., Boyce, M., Bettencourt, B. R., Hutabarat, R., Nochur, S., Vaishnaw, A., Gollob, J. *Mol. Ther.* **2017**, *25* (1), 71–78.
(142) Tanowitz, M., Hettrick, L., Revenko, A., Kinberger, G. A., Prakash, T. P., Seth, P. P. *Nucleic Acids Res.* **2017**, *45* (21), 12388–12400.
(143) Prakash, T. P., Graham, M. J., Yu, J., Carty, R., Low, A., Chappell, A., Schmidt, K., Zhao, C., Aghajan, M., Murray, H. F., Riney, S., Booten, S. L., Murray, S. F., Gaus, H., Crosby, J., Lima, W. F., Guo, S., Monia, B. P., Swayze, E. E., Seth, P. P. *Nucleic Acids Res.* **2014**, *42* (13), 8796–8807.

(144) Sardh, E., Harper, P., Balwani, M., Stein, P., Rees, D., Bissell, D. M., Desnick, R., Parker, C., Phillips, J., Bonkovsky, H. L., Vassiliou, D., Penz, C., Chan-Daniels, A., He, Q., Querbes, W., Fitzgerald, K., Kim, J. B., Garg, P., Vaishnaw, A., Simon, A. R., Anderson, K. E. *N. Engl. J. Med.* **2019**, *380* (6), 549–558.
(145) Nishina, K., Unno, T., Uno, Y., Kubodera, T., Kanouchi, T., Mizusawa, H., Yokota, T. *Mol. Ther.* **2008**, *16* (4), 734–740.
(146) Soutschek, J., Akinc, A., Bramlage, B., Charisse, K., Constien, R., Donoghue, M., Elbashir, S., Gelck, A., Hadwiger, P., Harborth, J., John, M., Kesavan, V., Lavine, G., Pandey, R. K., Racie, T., Rajeev, K. S., Röhl, I., Toudjarska, I., Wang, G., Wuschko, S., Bumcrot, D., Kotellansky, V., Limmer, S., Manoharan, M., Vornlocher, H. P. *Nature* **2004**, *432* (7014), 173–178.
(147) Khan, T., Weber, H., Dimuzio, J., Matter, A., Dogdas, B., Shah, T., Thankappan, A., Disa, J., Jadhav, V., Lubbers, L., Sepp-Lorenzino, L., Strapps, W. R., Tadin-Strapps, M. *Mol. Ther. - Nucleic Acids* **2016**, *5* (8), e342.
(148) Wolfrum, C., Shi, S., Jayaprakash, K. N., Jayaraman, M., Wang, G., Pandey, R. K., Rajeev, K. G., Nakayama, T., Charrise, K., Ndungo, E. M., Zimmermann, T., Koteliansky, V., Manoharan, M., Stoffel, M. *Nat. Biotechnol.* **2007**, *25* (10), 1149–1157.
(149) Li, G., Montgomery, J. E., Eckert, M. A., Chang, J. W., Tienda, S. M., Lengyel, E., Moellering, R. E. *Nat. Commun.* **2017**, *8* (1).
(150) Gmbh, S. B. H. *FASEB J.* **2016**, *5* (12), 1–23.
(151) Cheung, A., Bax, H. J., Josephs, D. H., Ilieva, K. M., Pellizzari, G., Opzoomer, J., Bloomfield, J., Fittall, M., Grigoriadis, A., Figini, M., Canevari, S., Spicer, J. F., Tutt, A. N., Karagiannis, S. N. *Oncotarget* **2016**, *7* (32), 52553–52574.
(152) Chen, C., Ke, J., Edward Zhou, X., Yi, W., Brunzelle, J. S., Li, J., Yong, E. L., Xu, H. E., Melcher, K. *Nature* **2013**, *500* (7463), 486–489.
(153) Appling, D. R. *FASEB J.* **1991**, *5* (12), 2645–2651.
(154) Toffoli, G., Cernigoi, C., Russo, A., Gallo, A., Bagnoli, M., Boiocchi, M. *Int. J. Cancer* **1997**, *74* (2), 193–198.
(155) Boogerd, L. S. F., Boonstra, M. C., Beck, A. J., Charehbili, A., Hoogstins, C. E. S., Prevoo, H. A. J. M., Singhal, S., Low, P. S., van de Velde, C. J. H., Vahrmeijer, A. L. *Oncotarget* **2016**, *7* (14), 17442–17454.
(156) Dohmen, C., Fröhlich, T., Lächelt, U., Röhl, I., Vornlocher, H. P., Hadwiger, P., Wagner, E. *Mol. Ther. Nucleic Acids* **2012**, *1* (1), e7.
(157) Lee, H., Lytton-Jean, A. K. R., Chen, Y., Love, K. T., Park, A. I., Karagiannis, E. D., Sehgal, A., Querbes, W., Zurenko, C. S., Jayaraman, M., Peng, C. G., Charisse, K., Borodovsky, A., Manoharan, M., Donahoe, J. S., Truelove, J., Nahrendorf, M., Langer, R., Anderson, D. G. *Nat. Nanotechnol.* **2012**, *7* (6), 389–393.
(158) Winkler, J. *Ther. Deliv.* **2013**, *4* (7), 791–809.
(159) Dassie, J. P., Liu, X. Y., Thomas, G. S., Whitaker, R. M., Thiel, K. W., Stockdale, K. R., Meyerholz, D. K., McCaffrey, A. P., McNamara, J. O., Giangrande, P. H. *Nat. Biotechnol.* **2009**, *27* (9), 839–846.
(160) McNamara, J. O., Andrechek, E. R., Wang, Y., Viles, K. D., Rempel, R. E., Gilboa, E., Sullenger, B. A., Giangrande, P. H. *Nat. Biotechnol.* **2006**, *24* (8), 1005–1015.
(161) Knerr, L., Prakash, T. P., Lee, R., Drury, W. J., Nikan, M., Fu, W., Pirie, E., Maria, L. De, Valeur, E., Hayen, A., Ölwegård-Halvarsson, M., Broddefalk, J., Ämmälä, C., Østergaard, M. E., Meuller, J., Sundström, L., Andersson, P., Janzén, D., Jansson-Löfmark, R., Seth, P. P., Andersson, S. *J. Am. Chem. Soc.* **2021**, *143* (9), 3416–3429.
(162) Kuo, C., Nikan, M., Yeh, S. T., Chappell, A. E., Tanowitz, M., Seth, P. P., Prakash, T. P., Mullick, A. E. *Nucleic Acid Ther.* **2022**, *32* (4), 300–311.
(163) Nikan, M., Tanowitz, M., Dwyer, C. A., Jackson, M., Gaus, H. J., Swayze, E. E., Rigo, F., Seth, P. P., Prakash, T. P. *J. Med. Chem.* **2020**, *63* (15), 8471–8484.
(164) Klabenkova, K., Fokina, A., Stetsenko, D. *Molecules* **2021**, *26* (17).

(165) Boisguérin, P., Deshayes, S., Gait, M. J., O'Donovan, L., Godfrey, C., Betts, C. A., Wood, M. J. A., Lebleu, B. *Adv. Drug Deliv. Rev.* **2015**, *87*, 52–67.
(166) Yin, H., Moulton, H. M., Seow, Y., Boyd, C., Boutilier, J., Iverson, P., Wood, M. J. A. *Hum. Mol. Genet.* **2008**, *17* (24), 3909–3918.
(167) Turner, J. J., Ivanova, G. D., Verbeure, B., Williams, D., Arzumanov, A. A., Abes, S., Lebleu, B., Gait, M. J. *Nucleic Acids Res.* **2005**, *33* (21), 6837–6849.
(168) Zakeri, B., Fierer, J. O., Celik, E., Chittock, E. C., Schwarz-Linek, U., Moy, V. T., Howarth, M. *PNAS* **2012**, *109* (12), E690-7.
(169) Sun, F., Zhang, W. Bin, Mahdavi, A., Arnold, F. H., Tirrell, D. A. *PNAS* **2014**, *111* (31), 11269–11274.
(170) Brune, K. D., Leneghan, D. B., Brian, I. J., Ishizuka, A. S., Bachmann, M. F., Draper, S. J., Biswas, S., Howarth, M. *Sci. Rep.* **2016**, *6*, 1–13.
(171) Österlund, T., Aho, A., Äärelä, A., Tähtinen, V., Korhonen, H., Virta, P. *Curr. Protoc. Nucleic Acid Chem.* **2020**, *83* (1), e122.
(172) Kiviniemi, A., Mäkelä, J., Mäkilä, J., Saanijoki, T., Liljenbäck, H., Poijärvi-Virta, P., Lönnberg, H., Laitala-Leinonen, T., Roivainen, A., Virta, P. *Bioconjug. Chem.* **2012**, *23* (9), 1981–1988.
(173) Luna Velez, M. V., Verhaegh, G. W., Smit, F., Sedelaar, J. P. M., Schalken, J. A. *Oncogene* **2019**, *38* (19), 3696–3709.
(174) An, F., Gong, B., Wang, H., Yu, D., Zhao, G., Lin, L., Tang, W., Yu, H., Bao, S., Xie, Q. *Apoptosis* **2012**, *17* (7), 702–716.
(175) Fang, Y., Judkins, J. C., Boyd, S. J., am Ende, C. W., Rohlfing, K., Huang, Z., Xie, Y., Johnson, D. S., Fox, J. M. *Tetrahedron* **2019**, *75* (32), 4307–4317.
(176) Geary, R. S., Norris, D., Yu, R., Bennett, C. F. *Adv. Drug Deliv. Rev.* **2015**, *87*, 46–51.
(177) Krishnamoorthy, K., Hoffmann, K., Kewalramani, S., Brodin, J. D., Moreau, L. M., Mirkin, C. A., Olvera De La Cruz, M., Bedzyk, M. J. *ACS Cent. Sci.* **2018**, *4* (3), 378–386.
(178) Gabizon, A., Horowitz, A. T., Goren, D., Tzemach, D., Shmeeda, H., Zalipsky, S. *Clin. Cancer Res.* **2003**, *9* (17), 6551–6559.
(179) Lindner, T., Loktev, A., Altmann, A., Giesel, F., Kratochwil, C., Debus, J., Jäger, D., Mier, W., Haberkorn, U. *J. Nucl. Med.* **2018**, *59* (9), 1415–1422.
(180) Zhang, Y., Xie, X., Yeganeh, P. N., Lee, D. J., Valle-Garcia, D., Meza-Sosa, K. F., Junqueira, C., Su, J., Luo, H. R., Hide, W., Lieberman, J. *PNAS* **2021**, *118* (9), e2022830118.
(181) Wan, Q., Zeng, Z., Qi, J., Zhao, Y., Liu, X., Chen, Z., Zhou, H., Zu, Y. *Cancers (Basel).* **2022**, *14* (6), 1570.
(182) Keinänen, O., Fung, K., Pourat, J., Jallinoja, V., Vivier, D., Pillarsetty, N. V. K., Airaksinen, A. J., Lewis, J. S., Zeglis, B. M., Sarparanta, M. *EJNMMI Res.* **2017**, *7*.
(183) Bargh, J. D., Isidro-Llobet, A., Parker, J. S., Spring, D. R. *Chem. Soc. Rev.* **2019**, *48* (16), 4361–4374.
(184) Moulder, S. L., Symmans, W. F., Booser, D. J., Madden, T. L., Lipsanen, C., Yuan, L., Brewster, A. M., Cristofanilli, M., Hunt, K. K., Buchholz, T. A., Zwiebel, J., Valero, V., Hortobagyi, G. N., Esteva, F. J. *Clin. Cancer Res.* **2008**, *14* (23), 7909–7916.

TURUN
YLIOPISTO
UNIVERSITY
OF TURKU

Painosalama Oy, Turku, Finland 2023

ISBN 978-951-29-9425-0 (Print)
ISBN 978-951-29-9426-7 (Online)
ISSN 0082-7002 (Print)
ISSN 2343-3175 (Online)